CRASHWORTHINESS STUDY FOR AUTOMOTIVE SEAT HEAD RESTRAINTS BY FINITE ELEMENT ANALYSIS WITH SIMPLIFIED SEAT MODEL AND LINEAR IMPACT TESTS

A THESIS SUBMITTED TO
THE GRADUATE SCHOOL OF NATURAL AND APPLIED SCIENCES
OF
MIDDLE EAST TECHNICAL UNIVERSITY

BY

ELIF EZGI AYTIMUR

IN PARTIAL FULFILLMENT OF THE REQUIREMENTS
FOR
THE DEGREE OF MASTER OF SCIENCE
IN
MECHANICAL ENGINEERING

JANUARY 2024

Approval of the thesis:

CRASHWORTHINESS STUDY FOR AUTOMOTIVE SEAT HEAD RESTRAINTS BY FINITE ELEMENT ANALYSIS WITH SIMPLIFIED SEAT MODEL AND LINEAR IMPACT TESTS

submitted by **ELIF EZGI AYTIMUR** in partial fulfillment of the requirements for the degree of **Master of Science in Mechanical Engineering Department, Middle East Technical University** by,

Prof. Dr. Halil Kalıpçılar
Dean, Graduate School of **Natural and Applied Sciences** _____

Prof. Dr. M. A. Sahir Arıkan
Head of Department, **Mechanical Engineering** _____

Prof. Dr. Mustafa İlhan Gökler
Supervisor, **Mechanical Engineering, METU** _____

Dr. Sevgi Saraç Karadeniz
Co-supervisor, **OTEST Company** _____

Examining Committee Members:

Prof. Dr. Ender Ciğeroğlu
Mechanical Engineering, METU _____

Prof. Dr. Mustafa İlhan Gökler
Mechanical Engineering, METU _____

Assoc. Prof. Dr. Ulaş Yaman
Mechanical Engineering, METU _____

Prof. Dr. S. Kemal İder
Mechanical Engineering, Çankaya University _____

Assist. Prof. Dr. Behzat Bahadır Kentel
Mechanical Engineering, Başkent University _____

Date:23.01.2024

I hereby declare that all information in this document has been obtained and presented in accordance with academic rules and ethical conduct. I also declare that, as required by these rules and conduct, I have fully cited and referenced all material and results that are not original to this work.

Name, Surname: Elif Ezgi Aytimur

Signature :

ABSTRACT

CRASHWORTHINESS STUDY FOR AUTOMOTIVE SEAT HEAD RESTRAINTS BY FINITE ELEMENT ANALYSIS WITH SIMPLIFIED SEAT MODEL AND LINEAR IMPACT TESTS

Aytimur, Elif Ezgi
M.S., Department of Mechanical Engineering
Supervisor: Prof. Dr. Mustafa İlhan Gökler
Co-Supervisor: Dr. Sevgi Saraç Karadeniz

January 2024, 108 pages

With the increase in the number of the traffic collisions, vehicle safety systems have gained importance. There is a wide variety of safety systems which have vital importance in the vehicles. Head restraints are important safety component in vehicles and must conform the requirements of Annex 6 of UN ECE R17 regulation by applying physical tests on the linear impact test system. Generally, the head restraints and seats manufacturers conduct Finite Element Analysis (FEA) of the head restraint together with the complex seat model which includes foams, covers, structural parts, joints, seat belt parts, functional parts, etc. In this thesis study, front and rear impact tests for the head restraints mounted on the bench type seat of light commercial vehicle have been realized on the linear impact test system in METU-BILTIR Center Vehicle Safety Unit according to Annex 6 of UN ECE R17. Based on the test results, a method to estimate result of the linear impact test of the head restraint is proposed by considering the complete head restraint model with the simplified seat model instead of the complex seat model. FEA for front and rear impact tests of the head restraint mounted on the simplified seat model are conducted. FEA results and linear impact test

results are compared, and they are in good agreement. It is shown that head restraint manufacturers can use this proposed method and can be confident about success of the head restraint in the linear impact tests beforehand.

Keywords: Head Restraint, Vehicle Seat, Crashworthiness, Vehicle Safety, Linear Impact Test

ÖZ

OTOMOTİV KOLTUK BAŞLIKLARI İÇİN BASİTLEŞTİRİLMİŞ KOLTUK MODELİ İLE SONLU ELEMANLAR ANALİZİ VE DOĞRUSAL DARBE TESTLERİ İLE ÇARPIŞMA DAYANIKLILIĞI ÇALIŞMASI

Aytimur, Elif Ezgi
Yüksek Lisans, Makina Mühendisliği Bölümü
Tez Yöneticisi: Prof. Dr. Mustafa İlhan Gökler
Ortak Tez Yöneticisi: Dr. Sevgi Saraç Karadeniz

Ocak 2024 , 108 sayfa

Trafik kazalarının artmasıyla birlikte, araç güvenlik sistemleri önem kazanmıştır. Araçlarda hayati öneme sahip birçok güvenlik sistemi bulunmaktadır. Koltuk başlıkları araçlardaki önemli güvenlik bileşenlerinden biridir ve doğrusal darbe test sisteminde uygulanan fiziksel testlerle UN ECE R17 Ek 6 gereksinimlerine uymak zorundadır. Genellikle koltuk başlığı ve koltuk üreticileri, kompleks koltuk modelini içeren koltuk başlığıyla birlikte Sonlu Elemenlar Analizi (SEA) gerçekleştirir; bu model sünger, kaplama, yapısal parçalar, eklemeler, emniyet kemeri parçaları, fonksiyonel parçalar vb. içerir. Bu tez çalışmasında, hafif ticari aracın bank tipi koltuğuna monte edilen koltuk başlıkları için ön ve arka çarpma testleri, ODTÜ-BİLTİR Merkezi Taşıt Güvenliği Birimi'ndeki doğrusal darbe test sisteminde UN ECE R17 Ek 6'ya göre gerçekleştirilmiştir. Test sonuçlarına dayanarak, kompleks koltuk modeli yerine basitleştirilmiş koltuk modeli ile birlikte tüm koltuk başlığı modeli doğrusal darbe testinin sonuçlarını tahmin etmek için yöntem olarak önerilmiştir. Basitleştirilmiş koltuk modeli üzerine monte edilen koltuk başlığının ön ve arka çarpma testleri için

SEA yapılmıştır. SEA sonuçları ile doğrusal darbe testi sonuçları karşılaştırılmış ve iyi bir uyum içindedir. Bu yöntemin koltuk başlığı üreticileri tarafından kullanılabileceği ve koltuk başlığı için doğrusal darbe testlerinin başarısında önceden güvenilebileceği gösterilmiştir.

Anahtar Kelimeler: Koltuk Başlığı, Araç Koltuğu, Çarpışma Dayanıklılığı, Taşıt Güvenliği, Doğrusal Darbe Testi

To my family and friends

ACKNOWLEDGMENTS

I am grateful to my supervisors Prof. Dr. Mustafa İlhan Gökler and Dr. Sevgi Saraç Karadeniz for their advice, support and encouragement throughout the study. It was a pleasure to know them and to work with them.

I would like to thank all personnel of METU-BILTIR Center Vehicle Safety Unit for their assistance during performing the linear impact tests.

I would like to thank Mr. Serdar Eren, General Manager, Mr. Bilal Bayır R&D Manager and Mr. Serhat İncesöz, R&D Center Responsible of Magna Seating Turkey for providing me valuable information.

I am also thankful to Kocaeli University Mechanical Engineering Department for their support.

Lastly, I would like to mention Numesys Company for their guideness and support about using ANSYS LS-DYNA.

I owe my deepest gratitude to my family and my friends for their support through my entire life.

TABLE OF CONTENTS

LIST OF TABLES

TABLES

LIST OF FIGURES

FIGURES

CHAPTER 1

INTRODUCTION

1.1. Introduction to Vehicle Safety

Vehicle safety started to be considered an important factor after the first recorded traffic accident in 1899 in New York City [1]. There have been three clear development periods in vehicle safety. The first development period started with understanding and correcting the improper conditions of the vehicle such as the blowout of the tires. Also, full-scale crash tests were started in the early 1930s. The second development period started with improving the components of the vehicle to avoid collision such as turning signals, headlamps, etc. Also, General Motors started a frontal crash test which was a collision of the vehicle to the barrier. Then, in 1956, seatbelts were developed, and it was a very important jump in vehicle safety for the early years. The third development period started with establishing vehicle safety standards. These standards are for clearing up the crashworthiness of vehicles, occupant safety, and collision avoidance.

USA, European countries and Japan are leading countries in terms of vehicle manufacturing and number of vehicles on the roads. In Handbook of Transport Systems and Traffic Control [2], general information about regulations are given. In USA, National Highway Traffic Administration (NHTSA) presented Federal Motor Vehicle Safety Standards (FMVSS). Likewise, in Europe, United Nations Economic Commission for Europe (UNECE) offered its own standards. Also, Japan has its own standards based on both UNECE and FMVSS. Detailed information about vehicle safety regulations will be given in Section 1.2.

In general, vehicle safety is classified into three categories which are active, passive and tertiary safety systems. A review of active and passive automotive safety systems to prevent the number of deaths and injuries due to traffic accidents is given in study of Vashist and Kumar [3].

A. Active Safety Systems

Active safety systems are used to prevent vehicle collisions and to avoid accidents. Some active safety systems warn the driver when sensing the accident potential such as lane departure, forward collision, blind spot detection, cross-traffic alert, etc. Some of the active safety systems affect the braking system for correcting situations and preventing accidents such as the anti-lock braking systems and electronic stability control. Using the parking sensors also prevents accidents.

B. Passive Safety Systems

"Crashworthiness" term is a related word that is used for the capability of vehicle structures to protect occupants when a crash happens, and crashworthiness of vehicles is important for the survivability of their occupants [1]. Passive safety systems are used to provide life-space for the occupants when a collision happens. The crumble zone helps to absorb the energy of impact before reaching the occupant. It is usually designed as located at the front and rear of the vehicle. It forms as a load path and most of the kinetic energy of impact can be absorbed by the components on the load paths. By these, life space for occupants is provided and the load is decreased [3, 4].

Passive safety systems also stop the harmful movability of occupants by restraint systems such as airbags, seat belts, head restraints and child restraint systems to reduce the risk of injury and death during a collision [3]. During a collision, an occupant has the energy to move forward while the vehicle stops suddenly like hitting the wall, and the airbag's aim is to absorb the occupant's kinetic energy which is attempted to move forward. It inflates in less than 50 milliseconds by filling with nitrogen gas. There are some airbag types and they are still being developed. They are usually called according to their location and purpose on vehicles like passenger and driver airbags as the frontal airbags, side airbags, knee airbags, etc. [5, 6].

When a frontal collision happens, seat belts are required for stopping the occupant who moves forward with its inertia to hit the steering wheel or dashboard of the vehicle. There are some types of seatbelts according to the way of fastening such as three-points, lap, and six-points seat belts. Three-point seat belts used in passenger cars are made of lap belt and shoulder belt which are for the pelvis and chest, respectively. The material of the seat belt is flexible therefore while the occupant moves forward, the seat belt expands a little bit to avoid harm [3]. An example of three-point seat belt is seen in Figure 1.1.

Vehicle seats are formed to provide comfort, but safety is also considered in their design. For example, it prevents sliding of occupants under the belt by handling the pelvis motion and also absorbing collision energy. Seats provide safety with their material properties and mechanisms inside. On the other hand, the safety performance of seats depend on head restraints and seat structure [7]. Head restraints, which are the main object of this thesis study, will be discussed in Section 1.3.

Figure 1.1. Three-point seat belt from [7]

C. Tertiary Safety Systems

Tertiary safety systems provide rescue information to rescue services such as ambulance, police, etc. just after the accident. Euro NCAP and International Association of Fire & Rescue Services (CTIF) developed a phone application which is called Euro Rescue, it is supposed to be used for all European countries [8].

1.2. Vehicle Safety Regulations

There are crashworthiness tests such as linear impact tests, static loading tests, sled tests, and full-scale tests for passive safety systems [1]. Linear impact tests, static loading tests and sled tests are applied for vehicle components. Apart from these three, full-scale tests are applied to full-body vehicles which is the last procedure for getting a safety approval before marketing. Crashworthiness tests are applied according to regulations which are called vehicle safety regulations. The regulations are mandatory procedures for improving the design and manufacturing of the vehicles. Those regulations are separated as local and universal and also, some vehicle manufacturers have their own regulations based on local or universal regulations. The most used regulations are the United Nations Economic Commission for Europe (UNECE) [9], Federal Motor Vehicle Safety Standards (FMVSS)[10], and the European New Car Assessment Program (Euro NCAP) [11].

NHTSA which is a US agency of safety in transportation enforces FMVSS. Regulations can be found on the NHTSA website [10]. There are some regulations for testing the crashworthiness of seats, head restraints, and seat anchorages such as

- FMVSS 202 Head Restraints for passenger vehicles
- FMVSS 207 Seating systems
- FMVSS 208 Occupant crash protection
- FMVSS 209 Seat belts assemblies
- FMVSS 213 Child restraint systems

After establishing FMVSS, NHTSA built the first New Car Assessment Program which is known as NCAP in 1979 for providing safer vehicles based on standards and informing the customer about the safety of the vehicles. The first test was done in May 1979 with a 35-mph front crash test proportional to NCAP and the test was based on FMVSS 208 which is for occupant protection [10]. After 1994, there was a rating system that provided easier to understand safety information and encouraged vehicle designers to build high-rating vehicles. In 1997, Euro NCAP was established

for Europe and also, there are many NCAP programs such as ANCAP for Australia and New Zealand, Latin NCAP for Latin America, C-NCAP for China, and J-NCAP for Japan [11, 12].

European vehicle safety standards are evaluated mainly by the European Union (EU) and the United Nations Economic Commission for Europe (UNECE). Regulations can be found on the UN ECE website [13]. Some UN ECE regulations which are related to seats, head restraints, and seat's anchorages, are

- UN ECE R14 Uniform provisions concerning the approval of vehicles with regard to safety-belt anchorages, ISOFIX anchorages systems and ISOFIX top tether anchorages
- UN ECE R16 Uniform provisions concerning the approval of:

  I. Safety-belts, restraint systems, child restraint systems and ISOFIX child restraint systems for occupants of power-driven vehicles

  II. Vehicles equipped with safety-belts, safety-belt reminders, restraint systems, child restraint systems and ISOFIX child restraint systems and i-Size child restraint systems
- UN ECE R17 Uniform provisions concerning the approval of vehicles with regard to the seats, their anchorages and any head restraints
- UN ECE R129 Uniform provisions concerning the approval of Enhanced Child Restraint Systems used on board of motor vehicles

The list of current regulations of different countries related to seats and head restraints can be found in Table 1.1.

Table 1.1. Regulations Related to the Seat and Head Restraint from [10, 13, 14]

	USA	EUROPE	CHINA
Head Restraints	FMVSS 202a	UN ECE R17	GB 11550-2009
Seats	FMVSS 207	UN ECE R17	GB 13057-2014
Seat Belts	FMVSS 209, 210	UN ECE R14, R16	GB 14166-2013
Child Restraint Systems	FMVSS 213	UN ECE R129	GB 14166-2013

In Turkey, UN ECE regulations are applied for vehicle safety tests and the thesis subject is about Annex 6 of UN ECE R17 Head Restraint Energy Dissipation which will be given in Chapter 2 and Chapter 3 in detail.

The Crash Test Dummies, which are also called Anthropomorphic Test Devices (ATDs), are used in the full-crash tests and the sled tests. The "impactors" which represent human body parts such as head, thorax, leg are used in linear impact tests. These will be explained in the following paragraphs.

ATDs are specific devices which are representation of human body as dimensional, weight proportional and they are used by researchers and manufacturers to understand human injuries during collisions [15]. There are various types of dummies according to their intended use, crash scenarios and also ages. The most commonly used ATDs are Hybrid III dummies which are used especially for the frontal impact tests. The Hybrid III dummy family with 50^{th} adult male, 95^{th} adult male and 5^{th} adult female dummy are widely used. According to percentile, crash test dummies are classified into three groups as 5^{th}, 50^{th} and 95^{th} based on their weight and size. For example, an average adult male is represented with 50^{th} percentile Hybrid III dummy. For more human-like characteristics in frontal impact tests instead of Hybrid III, THOR is developed by NHTSA [16, 17].

For the side impact tests, the first side impact dummy SID was developed according to the 50^{th} male without chest response in the late 1970s. Then, the BioSID dummy is developed by General Motors and the Society of Automotive Engineers (SAE) with a response of head, neck, shoulders, chest, abdomen and pelvis. In 1997, WorldSID was developed by the ISO based on medium size men for a more biofidelic side impact dummy. BioRID-II is a rear impact dummy which is improved to measure the response of the head and neck and it is used to prevent whiplash injuries during the rear impact [16, 17].

In the linear impact test system, ATDs are not used, instead "impactors" which represent parts of the human body are used. These impactors are Body Block, Upper Legform, Flexible Pedestrian Legform, Pedestrian Adult and Child Head Forms, Free Motion Head-form (FMH), Guided Head-form as shown in Figure 1.2 and Figure 1.3. "Body Block" impactor represents human thorax and it is used for impact tests of

driver against the steering mechanism. “Upper Legform” is used for evaluating injuries of upper leg and pelvis of the pedestrian in case of an accident. “Flexible Pedestrian Legform” represents human leg bones and is used for evaluating injuries of lower leg and knee in case of an accident. “Pedestrian Adult and Child Head Forms” are used for pedestrian safety tests to simulate head impact to the vehicle. Adult head-form has the mass of 4.5 kg and child head-form has the mass of 3.5 kg. “Free Motion Head-form” (FMH) impactor with the mass of 4.5 kg, is used for interior head impact in particular regions of vehicle such as pillar, side rail etc. and acceleration is evaluated by accelerometers inside the head-form. “Guided head-form” with the mass of 6.8 kg is used for evaluating energy dissipation of head restraint by accelerometers at the center of gravity of the head-form [15, 16].

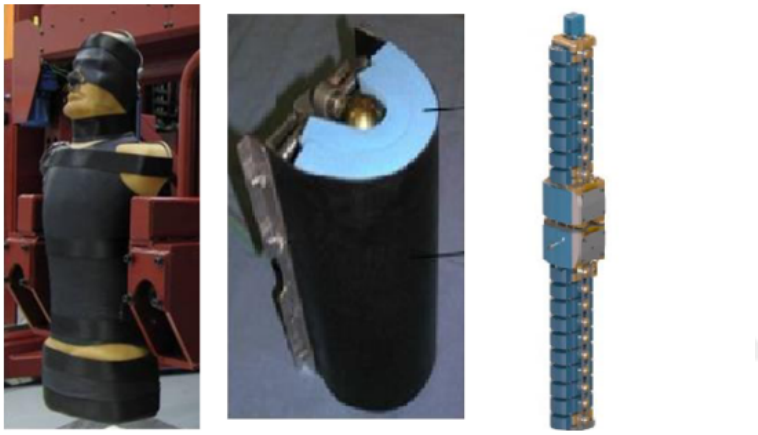

Figure 1.2. Body block, upper and flexible pedestrian legforms from [15, 16]

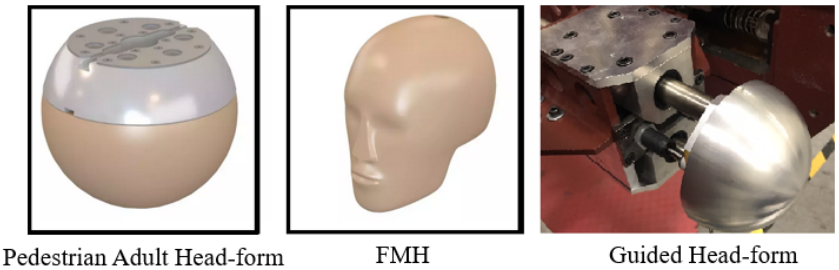

Figure 1.3. Pedestrian adult and child head-forms, FMH and guided head-form from [15]

1.3. Seats and Head Restraints

UN ECE defines the seat as a structure of a vehicle which has the purpose of comfort and limiting the occupant's harmful motion with a head restraint [18]. Seats are classified based on their position such as forward-facing seats, rearward-facing seats, side-facing seats and bench seats. Seat can be divided into three main parts: seat base(pan), seat-back and head restraint. These consists of other functional parts such as frame, padding, cover, suspension and reclining mechanisms [19, 20]. Each part has its role for safety and comfort. However, head restraint has a major effect on occupant safety with seat [7]. An example of a cut-view of the driver seat is seen in Figure 1.4. Head restraints may be described as integrated, detachable and separated. Integrated head restraint is assembled to seat-back whereas detachable and separated head restraints are designed independently from the seat. Detachable and separated head restraints have a different connection to the seat and to the vehicle, respectively [18]. In normal driving or when a collision happens, the seat has a significant effect on the safety and comfort of the occupant because they have continuous contact with each other.

Figure 1.4. Cut-view of driver seat from [20]

For safety, the main purpose of the seat and head restraint is to decrease the motion of the occupant's head and body as mentioned before. For that purpose, soft and energy-absorbing seat-back, active head restraints, and also seatbelt, airbags are still being developed [21]. Developments have progressed stage by stage. In the 1950s, front seats were designed as bench seat which was connected to each other. To determine the performance of the seat in a rear collision, performed crash tests for stronger and weaker seats to observe neck injury at General Motors Research Laboratories [22]. The head-neck support with increasing seatback height was also examined while there was no head restraint.

Head restraints first appeared in the 1960s to prevent injury caused by the motion between head and thorax but their safety performance was only 13-18%. The reason for the lower performance of the head restraint was that they were fixed and could not be arranged according to the occupant's height and position [23].

In 1969, NHTSA accepted the minimum height standard of head restraint which is 27.5" above the reference point of the seat in FMVSS 202 [24]. In an investigation into rear impact tests according to different seat strengths, Severy et al. provided establishing head restraints' standards [22]. They studied a 55-mph car-to-car crash test with %50 male driver and a seatback height of 28". They examined that the rigid seat reclined 41^{o} while the driver's head moved back from the top of the seatback. Then, in the 1970s, front seats were designed as bucket seats which had arrangements in fore-aft position and also in seatback angle. Also, head restraints were started to use as integrated or adjustable [22].

Head restraints must be positioned behind and close to occupants' heads for safety. Research Council for Automobile Repairs published head restraint positioning criteria which is used by the Insurance Institute for Highway Safety (IIHS) [25]. The criteria are divided into two. The first one describes the distance between the top of the occupant's head and the top of the head restraint. The second one describes the horizontal distance between the back of the occupant's head and the front of the head restraint (i.e. back-set distance). IIHS defines zones based on head restraint positioning such as good, acceptable, marginal, or poor [26]. Those zones are observed with biomechanical and observational studies and a good zone is described as a more

close distance between head and head restraint. IIHS zones are shown in Figure 1.5. As seen in the figure, in the “acceptable” zone, a head restraint is no farther than 8 cm below the top of the head and no farther than 9 cm behind it. When a head restraint is no farther than 6 cm below the top of the head and no farther than 7 cm behind it, it is considered as in “good” zone. These zones should be taken into account during the design of the head restraint and positioning of the occupant.

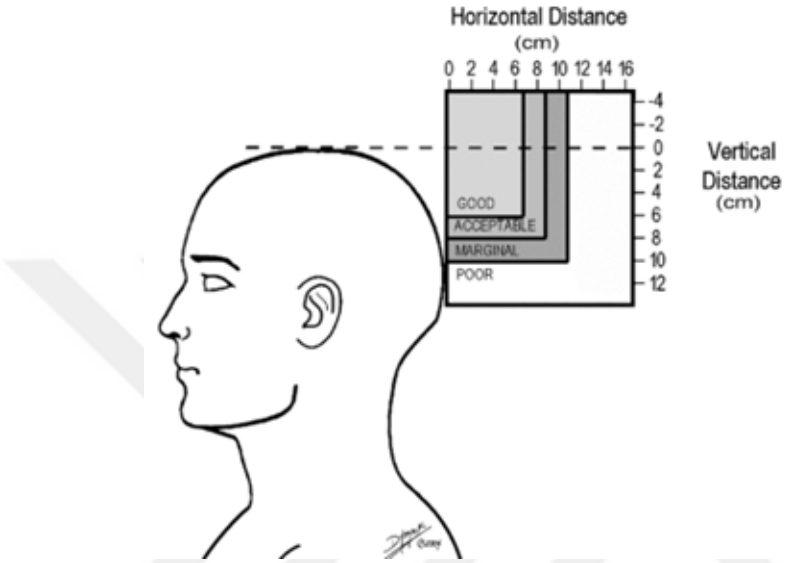

Figure 1.5. IIHS zones from [27]

Head restraints are important to prevent “whiplash” which is the most common type of neck injury and was identified as a neck injury by Crowe [28]. Most rear-end collisions with low velocity which is around 10 to 20 km/h cause whiplash. The impact can subject the head and neck to stresses that may exceed the neck’s limits and cause injury to the neck tissues. During the collision, the occupant’s body has a sharp motion to move rearward. This motion can be divided into four phases as shown in Figure 1.6. Phase 1 is called the "Retraction Phase". When the vehicle initially moves forward, the occupant’s back presses against the seat and the head remains stationary. This causes an abnormal S-shaped curve in the occupant’s neck. When the head reaches the maximum translation relative to the torso, phase 2 which is called the "Extension Phase" starts. The head rotates backwards into extension, and this causes significant shearing forces in the neck. Combination of shearing and compression forces in the neck can result in substantial injury. Phase 3 which is called "Rebound Phase" is started by making contact of the head to the head restraint. Phase

3 is the most critical phase of the whiplash event in terms of injury. The head makes contact with the head restraint and then rebounds forward. This rebound leads to the maximum head translational acceleration over all phases. After that, the seat belt stops the occupant's torso and the head moves forward freely. This starts Phase 4 which is called the "Protraction Phase". This forward movement of the head results in intense forward-bending motion of the neck. It can cause damage to muscles, spinal cord and brain. The phase ends when the head reaches its maximum forward translation relative to the torso.

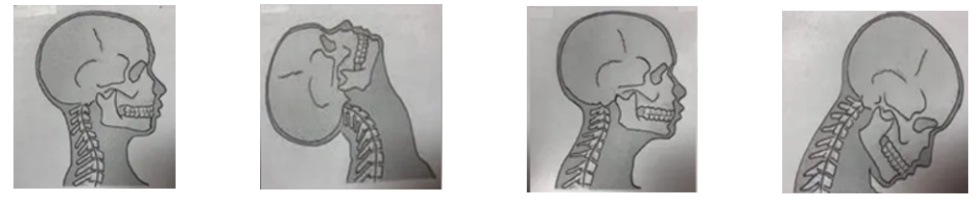

Figure 1.6. Four phases of the whiplash phenomena from [29]

It is shown that decreasing the neck injury risk can depend on limiting neck movement [26, 30]. Head restraints have a significant effect on preventing neck injury among other features of the vehicle [31]. To prevent whiplash, some seat and head restraint mechanisms have been attempted. For rear-end impact to control the rearward motion of the backrest, the WHIPS seat which is Volvo Whiplash Protection Study was developed [32]. It was to reduce the forward motion of occupants during the rebound phase and absorb the energy while reducing the distance between the occupant's head and head restraint. As a conclusion of the study, seat and head restraints were improved for whiplash with reclining and re-positioning, respectively.

The seat slide was improved by Schmitt et al. with a damping mechanism which was triggered by sensors [33]. When the sensor was activated, the seat moved approximately 40 millimeters to the back. The new seat slide system was approved by sled test with 16 km/h rear-impact. The new system reduced neck injury by almost 40%. With using a head restraint and recliner mechanism, the sliding mechanism is also used for reducing neck injury.

Lou and Zhou studied seat sliding mechanisms for preventing whiplash with a numerical model of BioRID II dummy used in MADYMO finite element analysis

program [34]. In the study, the seat sliding mechanism was improved by quasi-static tests and finite element simulations [35]. Then, Zhang and Zhou [36] improved the sliding mechanism developed by Lou and Zhou [35] and manufactured a prototype to test with the sled tests. The results of this study indicate that the sliding mechanism has a significant effect on preventing neck injury.

Özdemir et al. [37] performed a finite element model using the BioRID II dummy to observe the anti-whiplash injury mechanism. Different anti-whiplash mechanisms are developed and tested by sled test in METU-BILTIR Center Vehicle Safety Unit according to EuroNCAP whiplash test protocol. As a result of the study, the rapid anti-whiplash mechanism shows a positive effect on reducing whiplash injury.

Göçmen studied head restraint for effecting whiplash injury in METU-BILTIR Center Vehicle Safety Unit according to head restraint position and impact pulse [28]. EuroNCAP Whiplash Test Protocol is applied in sled test using Hybrid III 50^{th} percentile male adult crash dummy and light commercial vehicle driver seat. The results show that a closer position of the head restraint and the occupant's head decreases the whiplash injury potential.

To bring head and head restraint into contact in the first phase of the collision, active head restraints have been developed. Saab was the first one to introduce active head restraint in its model [38]. It was a mechanism which provided the application of upward and forward movement of the head restraint [21]. Mercedes-Benz developed active head restraint systems and it was called proactive head restraint system [39]. The system started to work by impact sensors and head restraint moved to upward and forward positions. Loughborough University improved active head restraint by calling smart head restraint in 2007 [39]. The system used twin ultrasonic sensors to identify the direction of the head and head restraint and the head restraint can be moved automatically to optimal upward and forward positions relative to the passenger's head. The new concept was developed as a combination of whiplash-mitigating head restraint and Volvo's system [31]. When a collision happens, both systems work together and this concept provides higher protection for a neck injury. Laban studied different commercial head restraints and developed a robust tracking system to provide proper positioning between the head restraint and the occupant's head while driving [40].

In the literature, limited studies related to energy dissipation of head restraint have been encountered. Chen et al. studied on energy absorption capability of head restraint [41]. According to China regulation, impact simulation was performed with LS-DYNA. Devkate and Navale [42] examined effect of different parameters on energy absorption of head restraint based on UN ECE R17 [19]. Naber and Carley [43] studied on different head restraint foam types to pass FMVSS 202a [24] requirements which is for energy absorption of head restraint.

1.4. Scope of the Thesis

In addition to the studies described in [28, 30], Doğan [4] examined load path of vehicle, Çöl [44] studied for evaluating child restraint system, Özden [45] studied about curtain airbags, Kaya [46] developed test procedure and fixture for ambulances and Karadeniz [16] studied about pedestrian protection in METU-BILTIR Center Vehicle Safety Unit. Although, linear impact tests are being realized for the head restraints in this center, there has not been any research study on head restraints.

The seat head restraint is important component for the occupant safety as discussed in the previous sections. In the industry, safety systems are improved by vehicle manufacturers with performing several computer analysis and physical tests on the linear impact test system. Finite Element Analysis (FEA) technique is commonly used in crashworthiness studies of automotive components. FEA of the particular head restraint is useful to estimate the test results before application of the physical tests which are costly. The head restraints developed by the manufacturer must conform the vehicle safety regulation before being used in the vehicle. Head restraint energy absorption capability tests are applied as the linear impact test based on Annex 6 of UN ECE R17 regulation [18]. In this thesis study, a method to estimate the result of the linear impact test of the head restraint is proposed by considering the complete head restraint model with the simplified seat model. By this way, complexity of the seat model, which requires intensive effort and causes consuming more times, will be avoided during the FEA. Therefore, FEA will consume less time and vehicle seat and head restraint manufacturer will be confident about success of the particular head restraint before applying the linear impact test and bearing the test costs.

In Chapter 2 and Chapter 3, experimental studies for front and rear impact tests of the head restraint, respectively are presented. Modelling of the seat head restraint with the simplified seat is described in Chapter 4. Finite Element Analyses for front and rear impact tests of the head restraint mounted on the simplified seat model are discussed in Chapter 5 and Chapter 6, respectively. The conclusion of the study and suggestions for the further studies are given in Chapter 7.

CHAPTER 2

EXPERIMENTAL STUDY ON LINEAR IMPACT TEST OF HEAD RESTRAINT FOR FRONT IMPACT

Seat head restraints endure various tests based on regulations to ensure occupant safety and, consequently, the comfort of the occupants. In this thesis, energy dissipation evaluation of head restraint is performed according to Annex 6 of UN ECE R17 regulation by linear impact test system. In this chapter, firstly Annex 6 of UN ECE R17 regulation for front impact is explained in Section 2.1. Test equipment, test devices and test specimen are introduced in Section 2.2 and Section 2.3, respectively. Preparation, performing, post-test and results of the front impact tests will be described according to the regulation by using the linear impact test system in following sections. Image processing of the high-speed video recorded during the front impact is also explained.

2.1. Front Impact Test in Annex 6 of UN ECE R17

UN ECE R17 regulation is related to strength of vehicle seats and their anchorages, design of the back parts of the seat, properties of head restraints and luggage impact [18]. The regulation is applied for the component in the vehicle type of M and N categories which are used for the occupant and load transport, respectively.

The tests defined in Annex 6 of this particular regulation are applied to the seats with head restraints for checking the head restraint's energy absorption. The related rules described in the regulation can be interpreted as follows:

- The tested seat must be securely attached and lockable in all designated positions.
- The head restraint should be positioned at most unfavourable position which is the highest level.
- For impact on the front face of the head restraint, the impact direction is horizontal. The impact point is given as 65 mm below the top of the head restraint.
- In the regulation, it is stated that approved equivalent test methods can be used instead of the pendulum. Therefore, the linear impact test system with the guided head-form can be used. The guided head-form has 165 mm in diameter and the mass of 6.8 kg.
- Head-form should impact the head restraint at a speed of 24.1 km/h.
- Head-form includes two accelerometers and a speed-measuring device.
- The deceleration/acceleration result is taken as the average of two accelerometers.
- The value of deceleration/acceleration of the head-form should not exceed 80g continuously over 3 milliseconds.
- No failure and break should be observed during the impact.

2.2. Test Equipment and Devices

In this thesis study, the Annex 6 of UN ECE R17 Energy Dissipation test procedure is applied to the manufacturer's head restraint. The test equipment used during the tests are given below:

a) Impact Test system:

METU-BILTIR Center Vehicle Safety Unit Linear Impact Test system is used. The head-form can be launched as guided or unguided by the linear impact test system. In the unguided impact, the head-form is launched by the system and hits the seat after the free flight stage. In a guided impact, the head-form stays connected to the rails of the launcher during the impact, it hits the head restraint at a specific speed and

rebounds. In this study, the tests are performed as guided impact. The head-form is accelerated by an electromagnetic system, and it can reach up to the speed of 42 km/h. The impact speed is adjusted according to the defined speed in the regulation [47]. The linear impact test system FronTone E-Liner in METU BILTIR Center Vehicle Safety Unit is seen in Figure 2.1.

Figure 2.1. Linear impact test system

b) Guided head-form:

It is a representation of the occupant's head for front and rear impacts on the head restraint and seat. Based on UN ECE R17 regulation, the outer diameter of the head-form should be 165 mm and mass of the head-form should be 6.8 kg.

In the linear impact test system, the head-form is half sphere combined with connection parts providing necessary mass and its material is aluminium. As stated by regulation, it strikes to head restraint with a speed of 24.1 km/h during the test. For different impact positions, strike points are changed related to the regulations and standards. Head-form is used as "impactor" seen in Figure 2.2.

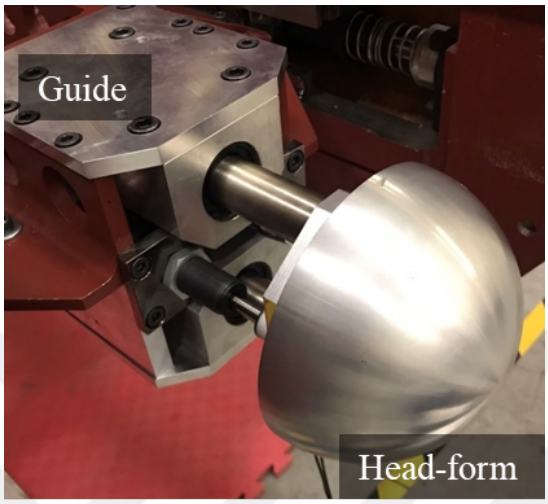

Figure 2.2. Guided head-form

c) Test computers:

Three test computers are used during the test. The first one is the linear impact test system test computer which is connected to the linear impact test system. By using this computer, the test type and test speed is defined to the system. The second computer is the sensors test computer. It is used for pre-test settings such as number and parameters of sensors in head-form and is also used for obtaining acceleration data at the end of the test. The third computer is the high-speed camera test computer. It is used for pre-test settings of cameras such as views, focus and zoom and is also used for obtaining recorded video at the end of the test.

d) Accelerometers inside the head-form:

There are two one-way accelerometers at the center of gravity of the head-form. Accelerometer measurements are recorded by the data acquisition system as acceleration versus time.

e) Twin-beams speed trap laser measurement system for speed measurement:

The speed of the impactor is input to the linear impact test system according to the speed defined in the Annex 6 of UN ECE R17 regulation [18].The impact speed is measured with a laser measurement system during the test for checking it. A twin-beams speed trap laser measurement system which works with cut-outs of the laser light, is used. The system composes of two boxes as the transmitter box and the receiver box. These two boxes are positioned such that the laser beams are in-line between the boxes located at sides of the test specimen as seen in Figure 2.3. The transmitter box delivers two beams parallel to each other and parallel to the horizontal plane as targeting to the receiver box. The distance between twin beams is constant and the laser system measures the time that the impactor passes between them and calculates the speed of the impactor.

Figure 2.3. Location of twin beams speed trap laser measurement system for the front impact

f) High-speed cameras:

The high-speed cameras record at 500 frames per second. One of the high-speed cameras is mounted on the crane system available in the test hole to record from the top. Another camera is placed side of the seat to record from the side. The high-speed cameras in the test hole are given in Figure 2.4.

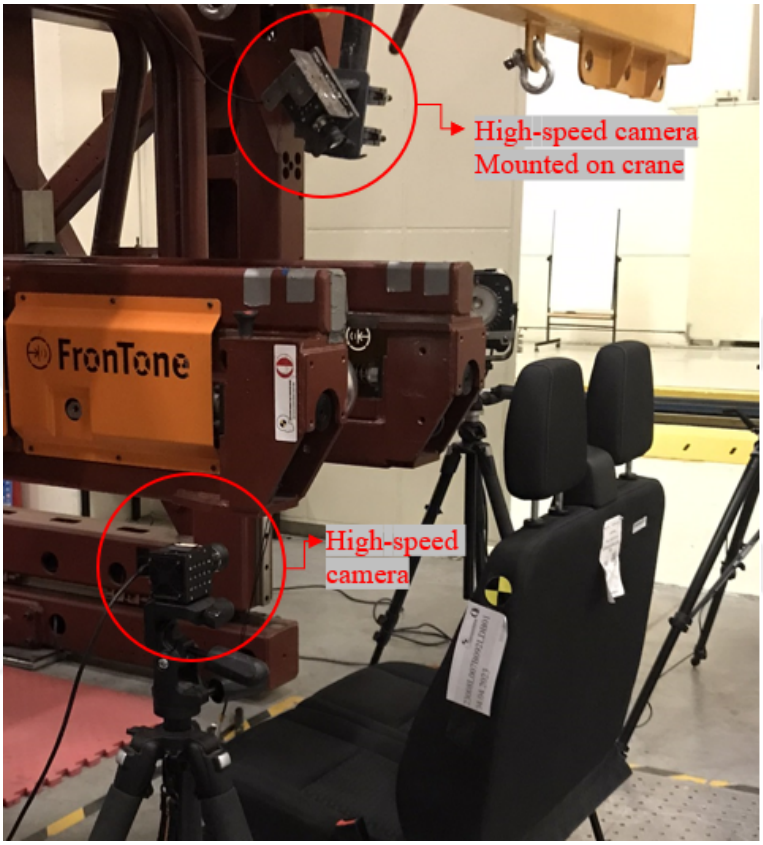

Figure 2.4. Location of the high-speed cameras for front impact in the test hole

g) Lights:

The seven lights are placed for the front impact as seen in Figure 2.5 to provide appropriate lighting conditions for the high-speed cameras. Four lights group are mounted on single stand while others have individual stands.

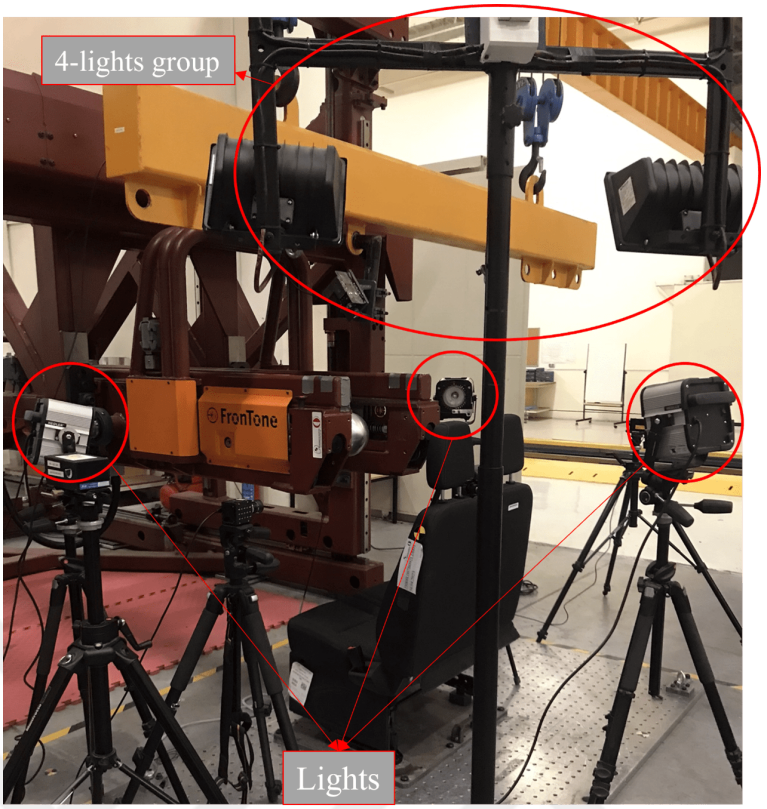

Figure 2.5. Lights placement for front impact in the test hole

h) Synchronizing the equipment and devices:

The test set-up for synchronizing activation of the launcher of the linear impact test system and triggering of cameras and sensors is required. This is also required for recording and transferring the data acquised during the test. This set-up is schematically shown in Figure 2.6. The linear impact test system test computer is connected to the linear impact test system by using plug “C” seen in Figure 2.7. This computer provides control on the system. The screen of this computer can be seen in Figure 2.8. By using the software of the linear impact test system test computer, the test type is defined as “guided head-form”, and the speed of impactor is input before starting the test. The data acquisition box for the sensors is connected to the linear impact test system by using plug “B” seen in Figure 2.7. Sensors in the head-form is connected to the data acquisition box for the sensors. The data acquisition box for sensors is powered externally. When the test is started on the linear impact test system, the data acquisition box for sensors simultaneously triggers sensors in the head-form. This box also records acceleration data during the test. After the test, the recorded acceleration

data is transferred to the sensors test computer from this box. The high-speed cameras box is connected to the linear impact test system by using plug “A” seen in Figure 2.7. The high-speed cameras box, which is powered externally, simultaneously triggers the camera-1 and camera-2 when the test is started on the linear impact test system. This box realises video recording during the test. After the test, the recorded videos are transferred to the high-speed cameras test computer.

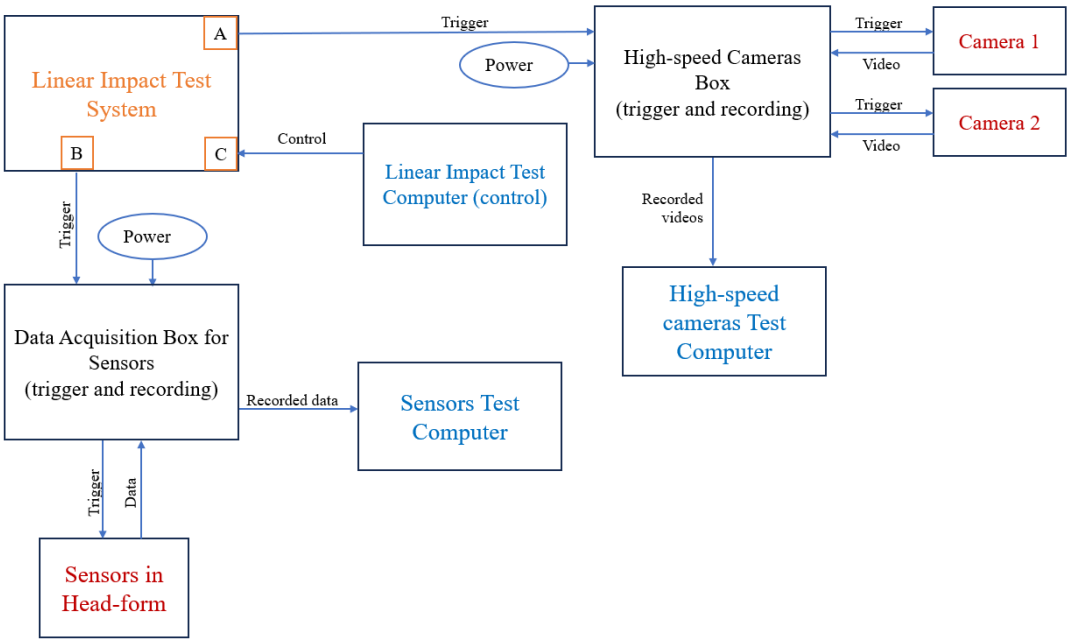

Figure 2.6. Schematical test set-up

Figure 2.7. Linear impact test system plugs

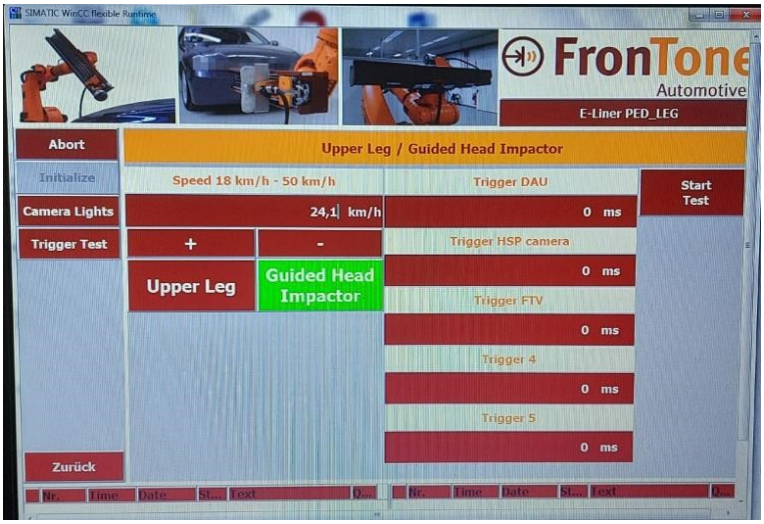

Figure 2.8. Screen of the linear impact test system test computer

h) Fixture Plate and Threaded Holes on the Floor of Test Hole:

The front impact test fixture which will be described in Section 2.4.1 is mounted to the aluminium fixture plate on floor of the test hole. This plate has size of 1400x2250 mm. As seen in Figure 2.9, there are several holes with M12 helicoils on the plate for securing the fixture and providing flexibility locating of the test specimen.

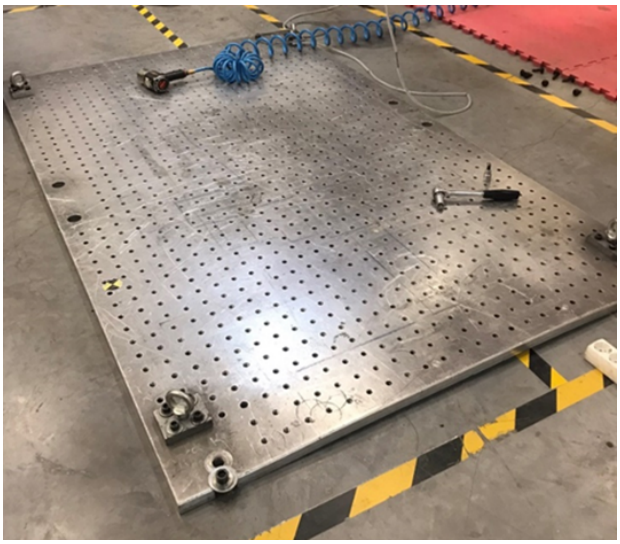

Figure 2.9. Aluminium fixture plate

There are fourteen threaded holes in the concrete floor of the test hole in the front of the linear impact test system. The threaded holes layout plan on the concrete floor of the test hole is given in Figure 2.10. The photograph given in Figure 2.11 shows

the threaded holes on the concrete floor and the linear impact test system. One of the threaded holes on the floor of the test hole and the bolt can be seen in Figure 2.12.

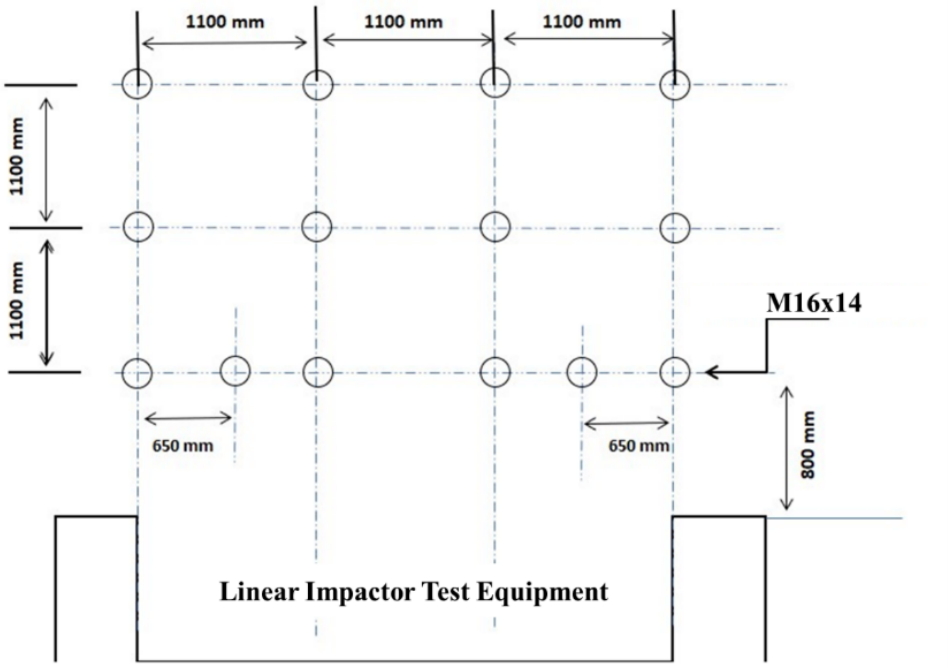

Figure 2.10. The threaded holes layout plan on the concrete floor of the test hole

Figure 2.11. The threaded holes on the concrete floor and the linear impact test system

Figure 2.12. One of the threaded holes on the floor and the used bolt

2.3. Test Specimen

The test specimen is the head restraint on a particular seat. The seat and head restraints are provided by the manufacturer. The seat is the front bench type passenger seat of a light commercial vehicle. The head restraint is locked in the seat as seen in Figure 2.13.

Figure 2.13. Test specimen

A typical head restraint is shown in Figure 2.14. Height of the head restraint is 219 millimetres and it has a trapezoidal shape. If the distance between the head restraint and the seat is adjustable, it should be locked to the highest point for the most unfavoured distance. For the locking of the head restraint into seat, head restraint has armature (red one) as seen in Figure 2.14 and Figure 2.15. The length of the leg of the armature at outside of the head restraint is 120 mm as seen in Figure 2.14. When the head restraint is locked, the distance between the top of the seat-back and the bottom of the head restraint is 37 mm as seen in Figure 2.16.

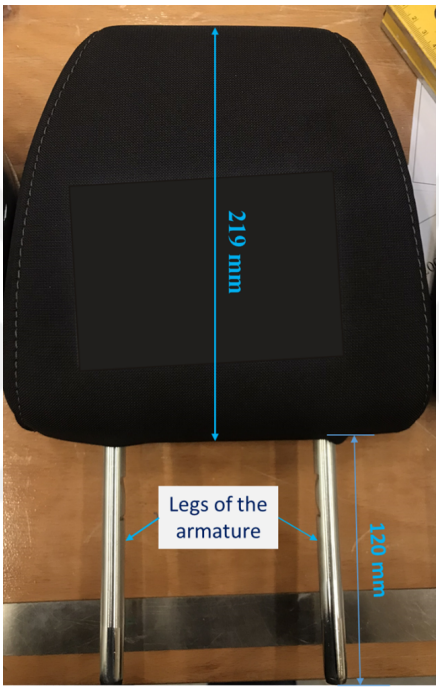

Figure 2.14. Length of the leg of the armature at outside of the head restraint

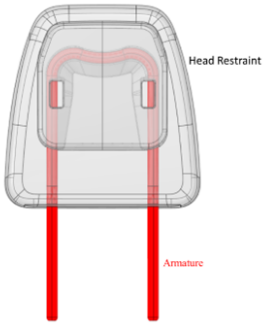

Figure 2.15. Armature (red one) in the head restraint

Figure 2.16. Distance between seat-back and head restraint

The manufacturer classifies the head restraints based on their mobility and shapes, designating those that move only in an upward-downward direction as two-way and those with the capability to fold as four-way. The type of head restraint changes the impact point of the rear impact test. In the case of a two-way head restraint, the impact point is the top of the head restraint, whereas for a four-way head restraint, it is the pivot of the head restraint.

2.4. Preparation for Front Impact Test of Head Restraint

According to the Annex 6 of UN ECE R17 regulation, the front impact test is applied on the linear impact test system with the guided head-form sub-system [18]. Before positioning of the launcher, the linear impact test system test computer is started, and the control cabin switch is on. System is initialized at horizontal position with "initialize" button. After the initialization, the system positioning is done such that the impact direction is parallel to the ground and the head-form hits the head restraint in horizontal direction. The test simulates rear impact to the vehicle. Thus, the foreside of the seat is placed in front of the impactor. A representation of the front impact on

head restraint is given in Figure 2.17. The guided head-form system shown in Figure 2.2, is mounted on the linear impact test system as seen in Figure 2.1, by fixing it to the end of the launcher. Axis of the guided head-form of the linear impact test system is arranged as parallel to the ground.

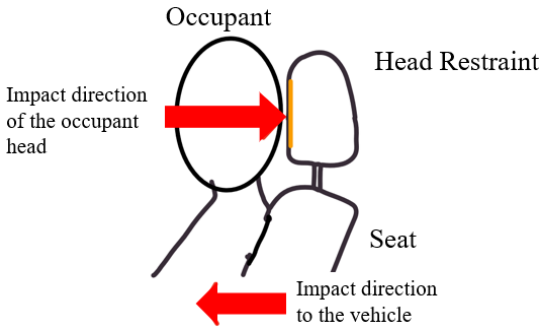

Figure 2.17. Representation of the front impact on head restraint

The test is repeated three times for accuracy in test results. For each test, the same type of head restraints which are provided by the manufacturer are used. After each test, the used head restraint is replaced with a new one. In the following subsections, preparation of the text fixture and test specimen, impact point marking, performing front impact test, post-test for front impact test will be explained.

2.4.1. Preparation of Text Fixture and Test Specimen

The front of the seat and the head restraint should be placed in front of the linear impact test system with the fixture. Test fixture is necessary for representing the vehicle floor that the seat is mounted. The front impact test fixture is shown in 2.18. As explained in the Section 2.2, the aluminium fixture plate is fixed to the floor of the test hole. The test fixture is located on the aluminium plate and the test specimen (i.e. head restraint mounted on the seat) is located on the text fixture of the front impact test as seen in Figure 2.18. Overall dimensions of the front impact test fixture is given in Appendix B. Depending on the seat structure, some seat mounting parts are required between the particular seat and the front impact test fixture.

Figure 2.18. Front impact test fixture for the linear impact test system

2.4.2. Impact Point Marking and Location of Trackers

The impact point is marked by the tracker on the head restraint as 65 mm below the head restraint's upper centre point. The impact point of the front impact test is seen in Figure 2.19.The tracker on the side of the seat-back is positioned such that the distance between axis of the joint in between seat-back and seat-bottom and center point of tracker is 500 mm as seen in Figure 2.20. The impact point of the head-form is marked on the head-form by paint as seen in Figure 2.21.

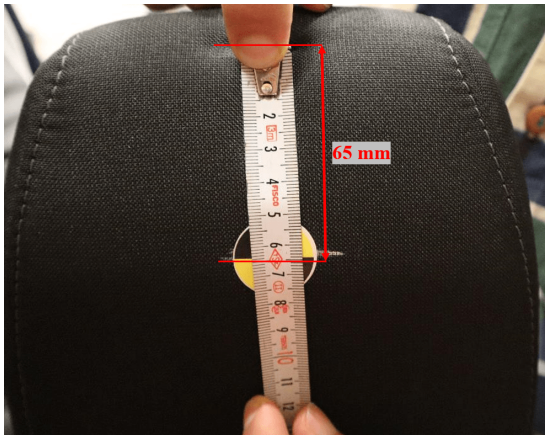

Figure 2.19. Impact point of the front impact test marked by the tracker on the head restraint

Figure 2.20. Positioning of the tracker on the side of the seat-back for the front impact test

Two reference trackers are sticked on the linear impact test system at a distance of 100 mm as shown in Figure 2.22. The aim of these reference trackers, which will be at the stationary positions during the test, is to convert the distance travelled by the tracker on the side of the seat-back from pixels to millimetres during image processing of the high-speed video.

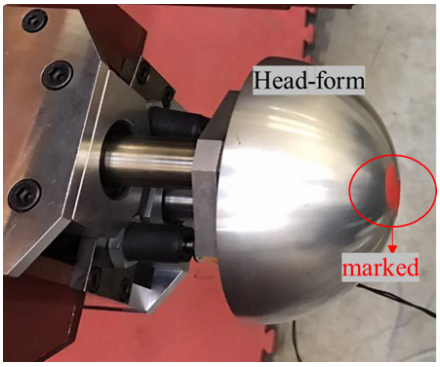

Figure 2.21. Marked head-form

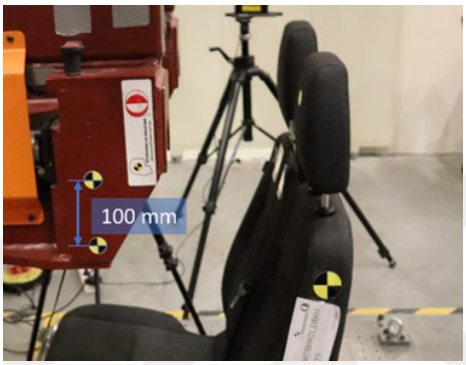

Figure 2.22. Reference trackers on the linear impact test system

2.5. Performing Front Impact Test of Head Restraint

After the test preparation has been completed as described in Section 2.4, the following steps are performed:

a) Before performing the test, the test set-up for synchronizing activation of the launcher of the linear impact test system and triggering of cameras and sensors which are described in Section 2.2 and Figure 2.6 should be checked.

b) In the linear impact test system test computer, the test type is selected as “guided head-form” as shown in Figure 2.8. The impact speed is input as 24.1 km/h according to the regulation.

c) Number of sensors and sensor parameters are defined in the sensors test computer.

d) In the high-speed cameras test computer, focus and zoom settings of the cameras are completed to cover the test zone.

e) Pre-test photographs of the seat, head restraint, and head-form are taken. Two sample photos are given in Figure 2.23 and Figure 2.24.

f) Lights are turned on.

g) Twin-beam speed laser system, which is described in Section 2.2, is turned on.

h) During the test, no one should be in the testing area, and objects that could cause damage should be removed from the testing area for safety. All the doors of the test hole are locked.

i) The warning lights in the test hole are turned on to indicate test is being performed.

j) From the linear impact test system test computer, the test is started with “Start Test” button on the screen of software of the linear impact test system. The accelerometers, the high-speed cameras and the linear impact test system are simultaneously triggered when the test is started.

k) During the test, videos are recorded by the high-speed cameras and acceleration data is also recorded.

Figure 2.23. Sample pre-test photo 1 of front impact test

Figure 2.24. Sample pre-test photo 2 of front impact test

2.6. Post-test for Front Impact Test of Head Restraint

After the test has been completed, the followings steps are applied:

a) The linear impact test system is deactivated by switching off the control cabin.

b) The measured impact speed of the head-form is checked during the test which is determined by the twin beam speed trap laser system. This system calculates the impact speed when head-form hits the head restraint and shows the value in its digital display.

c) The acceleration data of the sensors in head-form is transferred from the data acquisition box for sensors to the sensors test computer. The acceleration versus time curves are examined on this computer. The curves and data files are copied to an USB for further analysis.

d) The test videos recorded in the high-speed cameras box are transferred to the high-speed cameras test computer. The recorded videos are examined on this computer. Video recordings are copied to an USB for further analysis.

e) Post-test photographs of the head restraint and seat are taken. The sample post-test photo is seen in Figure 2.25.

f) Seat and head restraint are checked. There should be no failure and break on the seat and/or head restraint.

Figure 2.25. Sample post-test photo of front impact test

2.7. Result of Front Impact Tests

In this study, the front impact tests are applied three times with the same type of different head restraints for accuracy and repeatability. These tests are named as Test-1, Test-2, Test-3. According to the regulation described in Section 2.1, the value of deceleration/acceleration of the head-form should not exceed 80g continuously over 3 milliseconds. For all three tests, no failure on the head restraint and on the connection part between the seat and the head restraint has been observed.

In the following paragraphs, pre-test photos, post-test photos and Acceleration versus Time curves are given for each test. As described in Section 2.2, there are two accelerometers in the head-form. The data from these two accelerometers are recorded in the data acquisition box for sensors and transferred to the sensors test computer after each test. In obtaining the Acceleration versus Time curve, average of two acceleration

values at each time value is taken into account.

Results of Test-1

Pre-test photo for Test-1 is seen in Figure 2.26. No failure is observed for the head restraint and the seat. Post-test photos of Test-1 are seen in Figure 2.27. Acceleration versus Time curve is obtained as seen in Figure 2.28. The maximum acceleration of the head form is measured as 37.0g and the head restraint conforms with the regulation since it is less than 80g.

Figure 2.26. Pre-test photo for front impact Test-1

Figure 2.27. Post-test photos for front impact Test-1

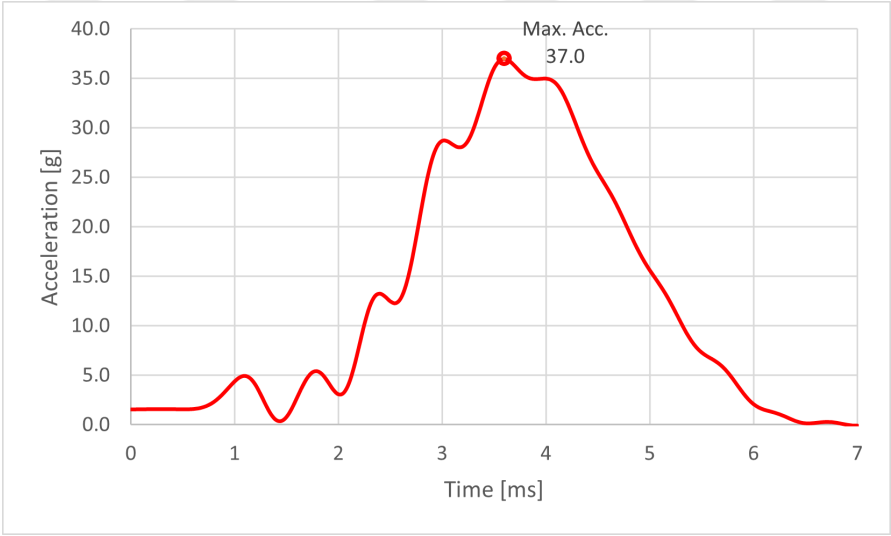

Figure 2.28. Acceleration vs Time curve for front impact Test-1

Results of Test-2

Pre-test photo for Test-2 is seen in Figure 2.29. No failure is observed for the head restraint and the seat. Post-test photos of Test-2 are seen in Figure 2.30. Acceleration versus Time curve is obtained as seen in Figure 2.31. The maximum acceleration of the head form is measured as 34.7g and the head restraint conforms with the regulation since it is less than 80g.

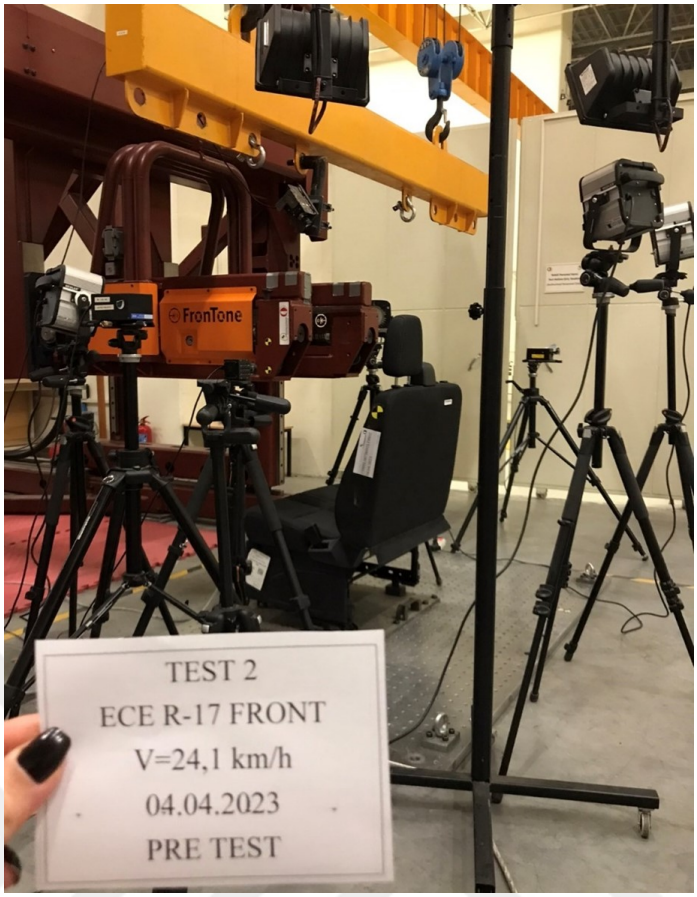

Figure 2.29. Pre-test photo for front impact Test-2

Figure 2.30. Post-test photos for front impact Test-2

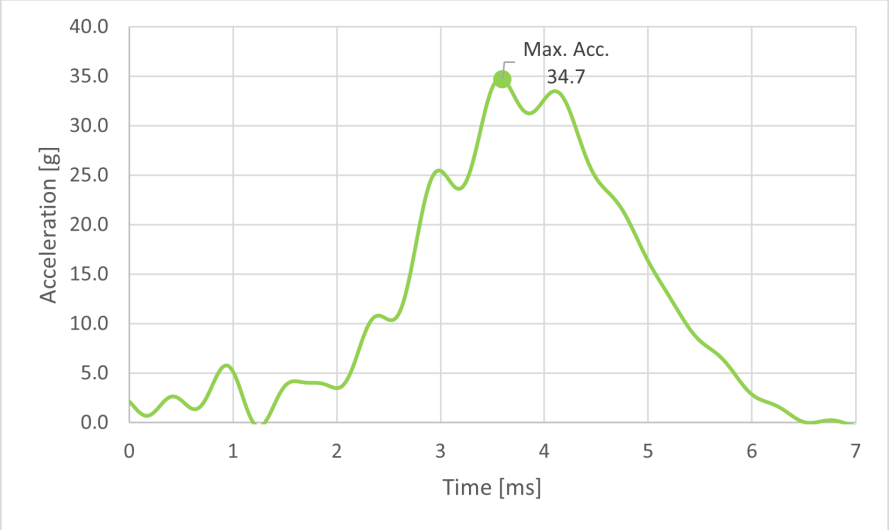

Figure 2.31. Acceleration vs Time curve for front impact Test-2

Results of Test-3

Pre-test photo for Test-3 is seen in Figure 2.32. No failure is observed for the head restraint and the seat. post-test photos of Test-3 are seen in Figure 2.33. Acceleration versus Time curve is obtained as seen in Figure 2.34. The maximum acceleration of the head form is measured as 34.5g and the head restraint conforms with the regulation since it is less than 80g.

Figure 2.32. Pre-test photo for front impact Test-3

Figure 2.33. Post-test photos for front impact Test-3

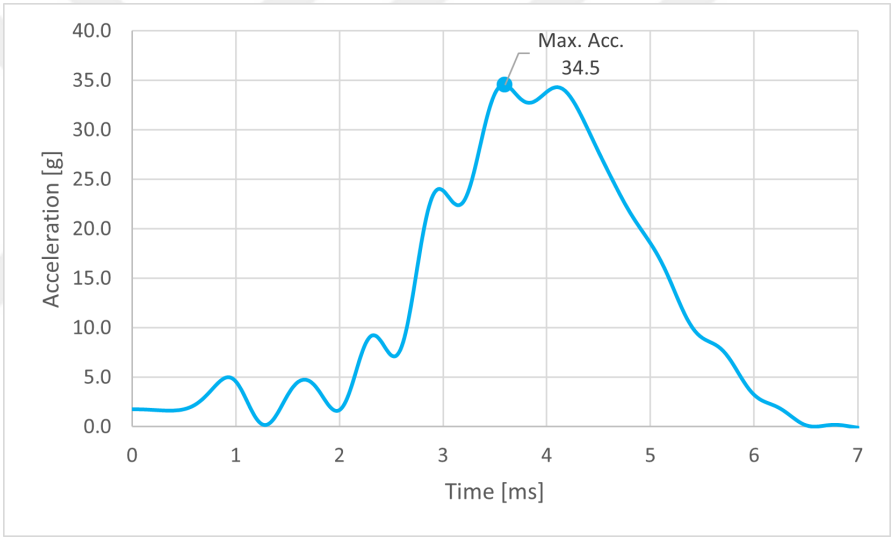

Figure 2.34. Acceleration vs Time curve for front impact Test-3

In Figure 2.35 Acceleration versus Time curves which are given in Figure 2.28, Figure 2.31 and Figure 2.34, are shown on the same figure. The main evaluation parameter of energy dissipation of the head restraint is the maximum acceleration of head form. Table 2.1 shows the test results. The average acceleration is 35.4g. The acceleration values show that head restraints can absorb most of the energy and the maximum acceleration values are smaller than 80g which conforms with the regulation [18]. Therefore, the typical head restraint is appropriate for the safety of occupant.

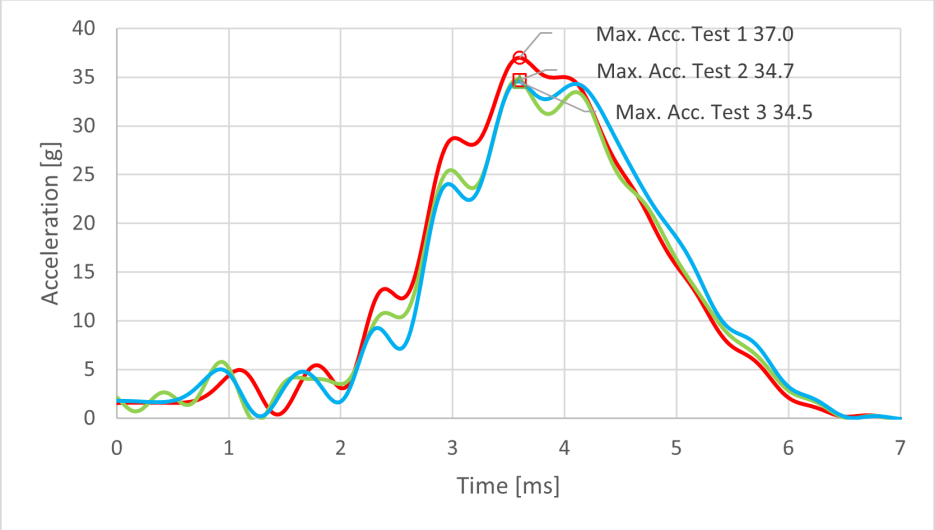

Figure 2.35. Acceleration curves for front impact tests

Table 2.1. Test results for the front impact

Test No	Maximum Acceleration
Test-1	37.0g
Test-2	34.7g
Test-3	34.5g

In commercial test application, the test report is prepared for the front impact test according to the Annex 6 of UN ECE R17 by using the results described above.

2.8. Image Processing of High-Speed Video Recorded During Front Impact Tests

The maximum displacement of the tracker on the side of the seat-back during the test is examined by using image processing software TEMA [48] after the test. The tracker is positioned at a distance of 500 mm from axis of the joint in between seat-back and seat-bottom as seen in Figure 2.20. The maximum displacement is determined by using the high-speed video of the side camera in the TEMA software. Positions of two reference trackers on the linear impact test system shown in Figure 2.22 and the tracker on the side of the seat-back is introduced to the software after tracker geometries are defined in the software as seen in Figure 2.36.

The followings are described in the software by referring to Figure 2.37:

- Distance between the two reference trackers on the linear impact system: 100 mm
- Perpendicular distance between the reference plane containing the two reference trackers on the linear impact system and the camera lens plane containing the lens of the high-speed camera on the side of the seat: 435 mm
- Distance between seat-back tracker plane containing the tracker on the side of the seat-back and the reference tracker plane: 180 mm

Then, the program measures the movement of the seat by monitoring the tracker point on the side of the seat-back. TEMA software has been used for video records of the Test-1, Test-2 and Test-3. By considering the results of these three tests, the average maximum displacement of the tracker is found as 50 mm for the front impact tests.

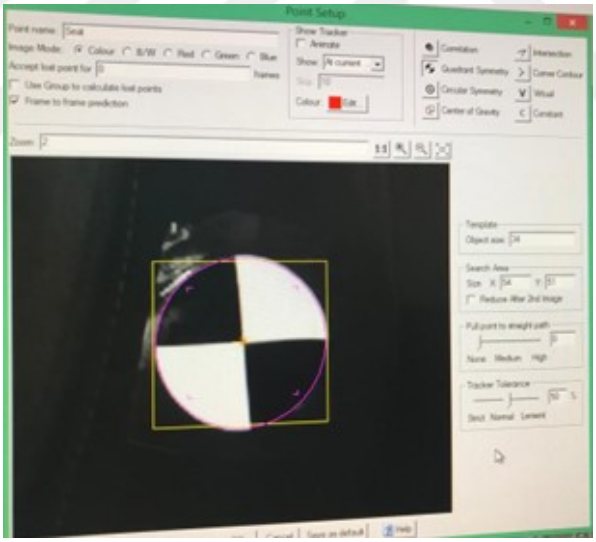

Figure 2.36. TEMA software screen

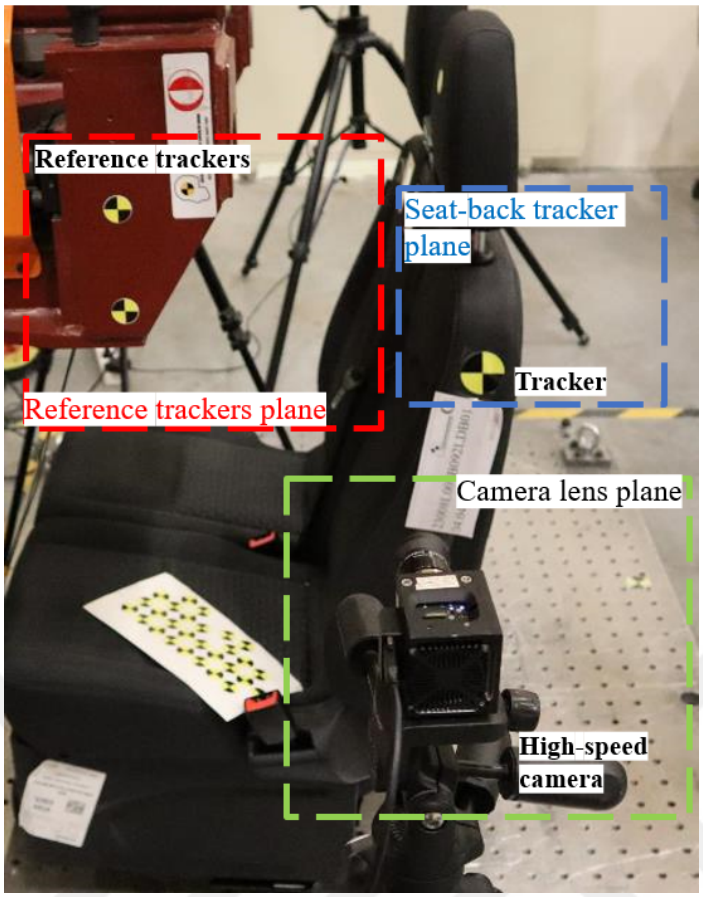

Figure 2.37. Planes for describing distances to the image processing software

CHAPTER 3

EXPERIMENTAL STUDY ON LINEAR IMPACT TEST OF HEAD RESTRAINT FOR REAR IMPACT

In this chapter, firstly, Annex 6 of UN ECE R17 regulation related to rear impact test of the head restraint is presented. The test equipment, test devices and test specimen have already been introduced in Chapter 2. However, there are some differences in rear impact tests. Preparation and performing of the rear impact test, post-test, and results of rear impact test are presented in the following sections. Image processing of the high-speed video recorded during the rear impact is also discussed.

3.1. Rear Impact Test in Annex 6 of UN ECE R17

The related rules in Annex 6 of UN ECE R17 [18] for the rear impact test can be interpreted as follows:

- The tested seat must be securely attached and lockable in all designated positions.
- The head restraint should be positioned at most unfavourable position which is the highest level.
- For impact on the rear face of the head restraint, the direction of impact is 45^{o} angle from the vertical and the impact point is the top of the head restraint.
- In the regulation, it is stated that approved equivalent test methods can be used instead of the pendulum. Therefore, the linear impact test system with the guided head-form can be used. The guided head-form has 165 mm in diameter and the mass of 6.8 kg.

- Head-form should impact the head restraint at a speed of 24.1 km/h.
- Head-form includes two accelerometers and a speed-measuring device.
- The deceleration result is taken as the average of two accelerometers.
- The value of deceleration of the head-form should not exceed 80g continuously over 3 milliseconds.
- No failure and break should be observed during the impact.

3.2. Preparation for Rear Impact Test of Head Restraint

According to the Annex 6 of UN ECE R17 regulation, the rear impact test is applied on the linear impact test system with the guided head-form system. Based on the regulation, the head-form hit the top of the head restraint with a 45^o angle as seen in Figure 3.1 . The launcher of the available linear impact test system does not allow 45° angle with respect to horizontal plane due to the limiting rotation of the launcher at the impact point height. Thus, 15° is provided by positioning the launcher of linear impactor system as seen in Figure 3.2 and 30° is provided by the rear impact test fixture which is shown in Figure 3.3 and Appendix B. By this way, 45° angle is provided. Geometric verification of this for the rear impact is shown in Figure 3.4.

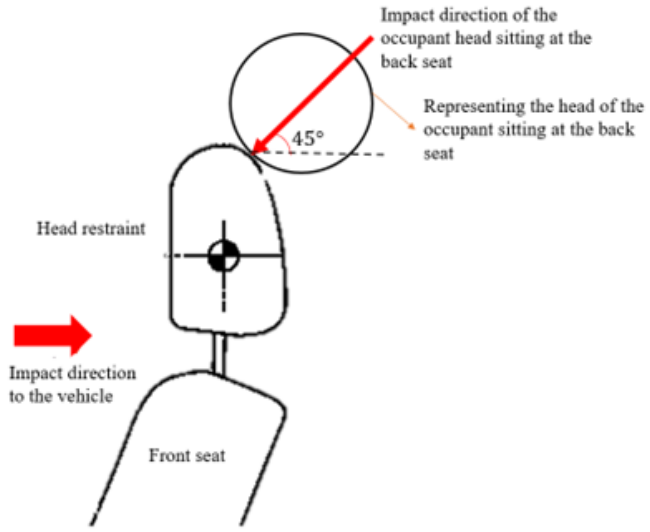

Figure 3.1. Representation of the rear impact on head restraint

This rear linear impact test simulates impact of the head of the occupant seating at the back seat to the head restraint mounted on the front seat during the front impact to the vehicle. Thus, the back side of the seat is placed in the front of the impactor and the impact direction of the head-form simulates the rear-seat occupant's head motion. The guided head-form system (Figure 2.2) is mounted on the linear impact test system (Figure 2.1) by fixing it to the end of the launcher. The test is repeated three times for accuracy in test results. For each test, the same type of head restraints which are provided by the manufacturer are used. After each test, the used head restraint is replaced with a new one. In the following subsections, the test preparation, performing tests and post-test activities are presented.

Figure 3.2. 15° angle of the launcher

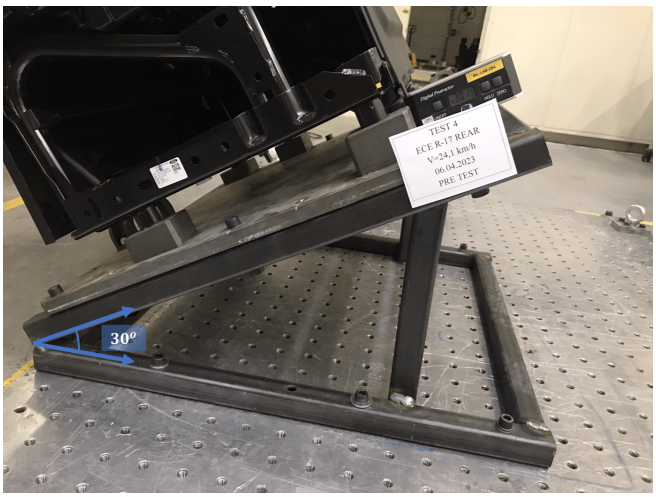

Figure 3.3. 30° angle of rear impact test fixture

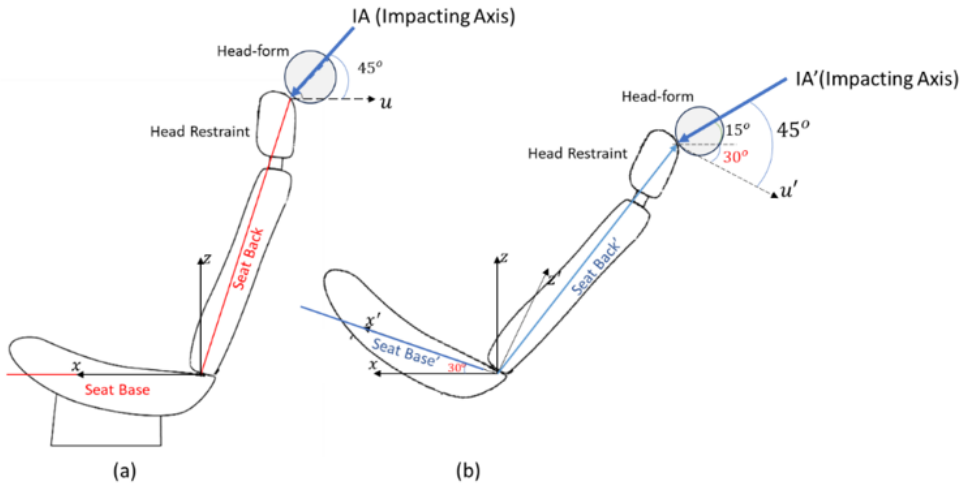

Figure 3.4. Geometric verification of the fixture set-up for the rear impact (a) the set-up described in UN ECE R17 Annex 6 (b) the set-up arranged for the tests conducted during the thesis study

3.2.1. Preparation of the text fixture and test specimen

The back side of the seat-back and the head restraint are placed in front of the linear impact test system with the rear impact test fixture. The rear impact test fixture is necessary for correct positioning as described in Figure 3.4 and representing the vehicle floor that the seat is mounted on. As explained in Section 2.2, the aluminium fixture plate is fixed to the floor of the test hole. The rear impact test fixture is located on the aluminium plate and the test specimen (i.e. head restraint mounted on the seat) is located on the rear impact test fixture together with some seat mounting parts as seen in Figure 3.5.

3.2.2. Placement of the Test Devices

Working principle of the twin-beams speed trap laser measurement system has already been given in Chapter 2. In the rear impact, two boxes of the system are located at 15° angle relative to horizontal plane due to the impact direction as seen in Figure 3.6. The seven lights are placed for the rear impact as seen in Figure 3.7. High-speed cameras, which are described in Chapter 2, are located for the rear impact as seen in Figure 3.8.

Figure 3.5. Rear impact test fixture

Figure 3.6. Location of twin beams speed trap laser measurement system for rear impact test

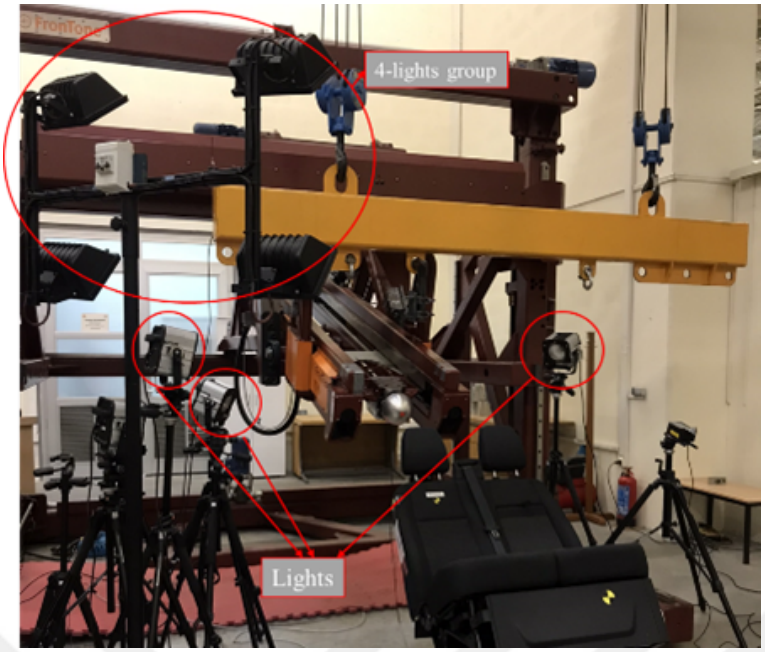

Figure 3.7. Lights placement for rear impact test in the test hole

Figure 3.8. Location of the high-speed cameras for rear impact in the test hole

3.2.3. Impact Point Marking and Location of Trackers

The impact point is marked by the tracker at the centre of the top of the head restraint as seen in Figure 3.9.The tracker on the side of the seat-back is positioned such that the distance between axis of the joint in between seat-back and seat-bottom and center point of tracker is 500 mm as seen in Figure 3.10. The impact point of the head-form is marked on the head-form by paint as seen in Figure 2.21 and two reference trackers are sticked on the linear impact system at a distance of 100 mm as shown in Figure 2.22 in Chapter 2.

Figure 3.9. Impact point of the rear impact test and tracker on the head restraint

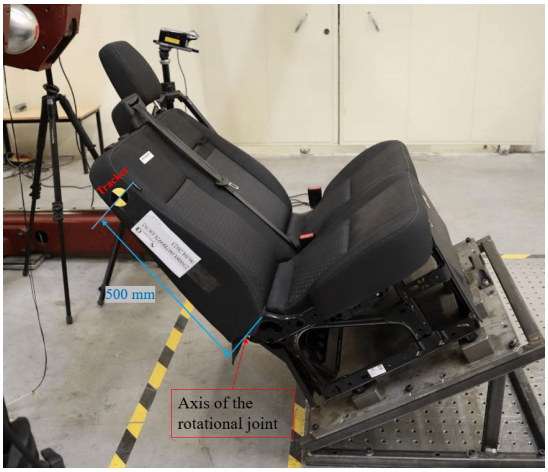

Figure 3.10. Positioning of the tracker on the side of the seat-back for the rear impact test

3.3. Performing Rear Impact Test of Head Restraint

After the test preparation has been completed as described in Section Section 3.2, the following steps are performed:

a) Before performing the test, the test set-up for synchronizing activation of the launcher of the linear impact test system and triggering of cameras and sensors which are described in Section 2.2 and Figure 2.6 should be checked.

b) In the linear impact test computer, the test type is selected as “guided head-form”. The impact speed is input as 24.1 km/h according to the regulation.

c) Number of sensors and sensor parameters are defined in the sensors test computer.

d) In the high-speed cameras test computer, focus and zoom settings of the cameras are completed to cover the test zone.

e) Pre-test photographs of the seat, head restraint, and head-form are taken. Two sample photos are given in Figure 3.11 and Figure 3.12.

f) Lights are turned on.

g) Twin-beam speed laser system is turned on.

h) During the test, no one should be in the testing area, and objects that could cause damage should be removed from the testing area for safety. All the doors of the test hole are locked.

i) The warning lights in the test hole are turned on to indicate test is being performed.

j) From the linear impact test system test computer, the test is started with “Start Test” button on the screen of software of the linear impact test system. The accelerometers, the high-speed cameras and the linear impact test system are simultaneously triggered when the test is started.

k) During the test, videos are recorded by the high-speed cameras and acceleration data is also recorded.

Figure 3.11. Sample pre-test photo 1 of rear impact test

Figure 3.12. Sample pre-test photo 2 of rear impact test

3.4. Post-test for Rear Impact Test of Head Restraint

After the test has been completed, the followings steps will be applied:

a) The linear impact test system is deactivated by switching off the control cabin.

b) The measured impact speed of the head-form is checked during the test which is determined by the twin beam speed trap laser system. This system calculates the impact speed when head-form hits the head restraint and shows the value in its digital display.

c) The acceleration data of the sensors in head-form is transferred from the data acquisition box for sensors to the sensors test computer. The acceleration versus time curves are examined on this computer. The curves and data files are copied to an USB for further analysis.

d) The test videos recorded in the high-speed cameras box are transferred to the high-speed cameras test computer. The recorded videos are examined on this computer. Video recordings are copied to an USB for further analysis.

e) Post-test photographs of the head restraint and seat are taken. The sample post-test photo is seen in Figure 3.13.

f) Seat and head restraint are checked. There should be no failure and break on the seat and/or head restraint.

Figure 3.13. Sample post-test photo of rear impact test

3.5. Result of Rear Impact Tests

In this study, the front impact tests are applied three times with the same type of different head restraints for accuracy and repeatability. These tests are named as Test-4, Test-5, Test-6. According to the regulation described in Section 3.1, the value of deceleration/acceleration of the head-form should not exceed 80g continuously over 3 milliseconds. For all three tests, no failure on the head restraint and on the connection part between the seat and the head restraint has been observed.

In the following paragraphs, pre-test photos, post-test photos and Acceleration versus Time curves are given for each test. Similar to the front impact test, average of two acceleration values at each time value is taken into account in obtaining Acceleration versus Time curve.

Results of Test-4

Pre-test photo for Test-4 is seen in Figure 3.14. No failure is observed for the head restraint and the seat. Post-test photos of Test-4 are seen in Figure 3.15. Acceleration versus Time curve is obtained as seen in Figure 3.16. The maximum acceleration of the head form is measured as 35.4 and the head restraint conforms with the regulation since it is less than 80g.

Figure 3.14. Pre-test photo for rear impact Test-4

Figure 3.15. Post-test photos for rear impact Test-4

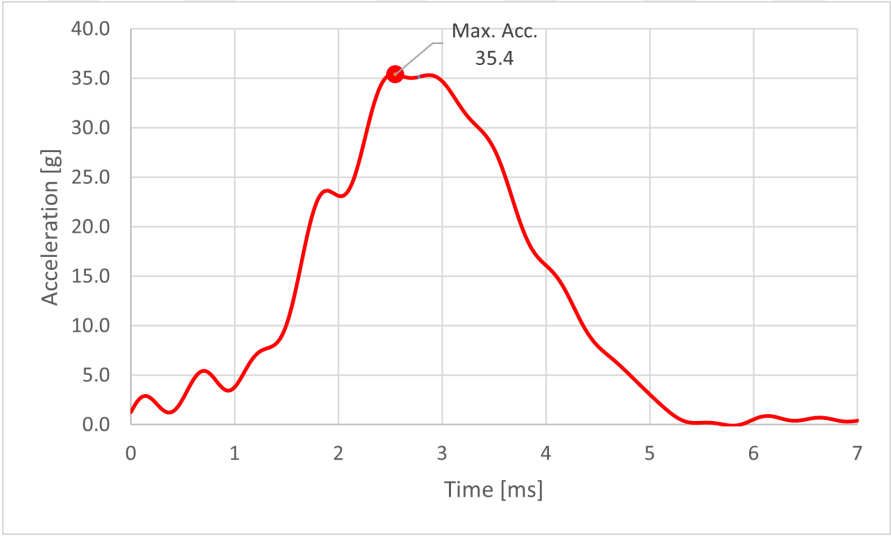

Figure 3.16. Acceleration vs Time curve for rear impact Test-4

Results of Test-5

Pre-test photo for Test-5 is seen in Figure 3.17. No failure is observed for the head restraint and the seat. Post-test photos of Test-5 are seen in Figure 3.18. Acceleration versus Time curve is obtained as seen in Figure 3.19. The maximum acceleration of the head form is measured as 33.6 and the head restraint conforms with the regulation since it is less than 80g.

Figure 3.17. Pre-test photo for rear impact Test-5

Figure 3.18. Post-test photos for rear impact Test-5

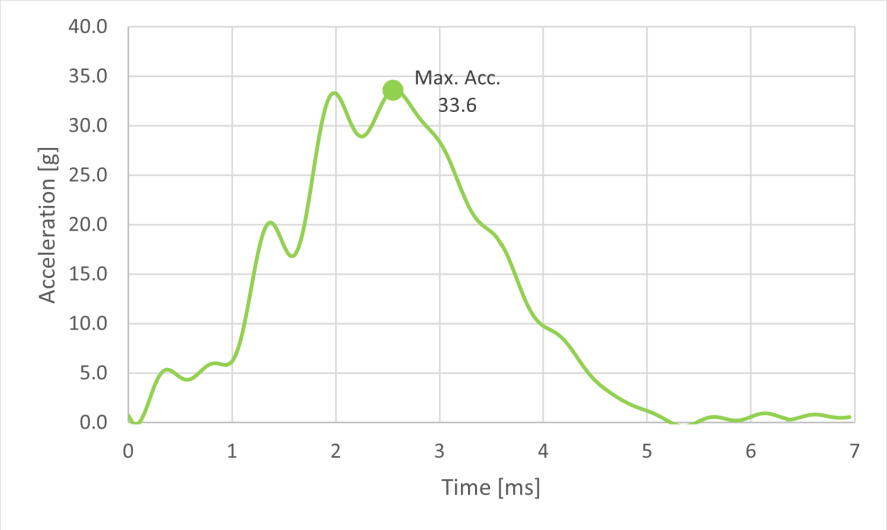

Figure 3.19. Acceleration vs Time curve for rear impact Test-5

Results of Test-6

Pre-test photo for Test-6 is seen in Figure 3.20. No failure is observed for the head restraint and the seat. Post-test photos of Test-6 are seen in Figure 3.21. Acceleration versus Time curve is obtained as seen in Figure 3.22. The maximum acceleration of the head form is measured as 35.1 and the head restraint conforms with the regulation since it is less than 80g.

Figure 3.20. Pre-test photo for rear impact Test-6

Figure 3.21. Post-test photos for rear impact Test-6

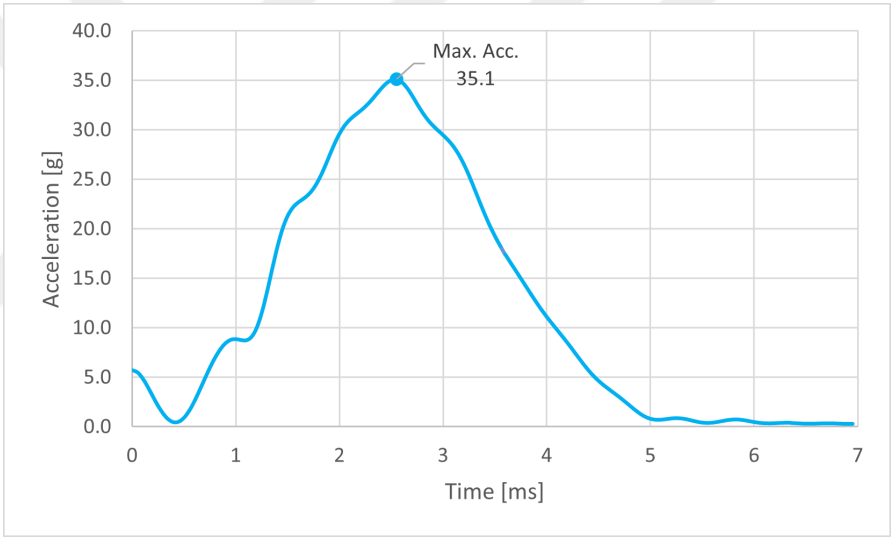

Figure 3.22. Acceleration vs Time curve for rear impact Test-6

In Figure 3.23 Acceleration versus Time curves which are given in Figure 3.16, Figure 3.19 and Figure 3.22, are shown on the same figure. The main evaluation parameter of energy dissipation of the head restraint is the maximum acceleration of head form. Table 3.1 shows the test results. The average acceleration is 34.7g. The acceleration values show that head restraints can absorb most of the energy and the maximum acceleration values are smaller than 80g which conforms with the regulation [18]. Therefore, the typical head restraint is appropriate for the safety of occupant.

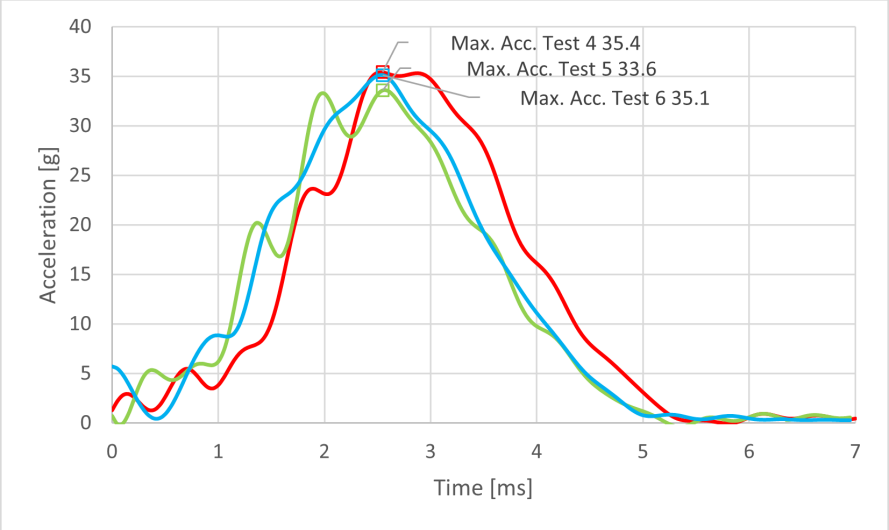

Figure 3.23. Acceleration curves for rear impact tests

Table 3.1. Test results for the rear impact

Test No	Maximum Acceleration
Test-4	35.4g
Test-5	33.6g
Test-6	35.1g

In commercial test application, the test report is prepared for the rear impact test according to the Annex 6 of UN ECE R17 by using the results described above.

3.6. Image Processing of the High-Speed Video Recorded During Rear Impact Tests

Using the image processing software TEMA has already been described in Chapter 2. The followings are described in the software by referring to the planes shown in Figure 2.37:

- Distance between the two reference trackers on the linear impact system: 100 mm

- Perpendicular distance between the reference plane containing the two reference trackers on the linear impact system and the camera lens plane containing the lens of the high-speed camera on the side of the seat: 585 mm
- Distance between seat-back tracker plane containing the tracker on the side of the seat-back and the reference tracker plane: 180 mm

The maximum displacement of the seat is calculated 15 mm for the rear impact tests.

CHAPTER 4

MODELLING OF SEAT HEAD RESTRAINT WITH SIMPLIFIED SEAT

The linear impact test according to the Annex 6 of UN ECE R17 is costly. Before sending the head restraint to the test facilities, Finite Element Analysis (FEA) technique is commonly used in crashworthiness studies of head restraint. Using the complete model of the head restraint together with complete model of the vehicle seat is time consuming in FEA studies. In this thesis study, a method to estimate the result of the linear impact test of the head restraint is proposed by considering head restraint with the simplified seat model. By this way, complexity of the seat model will be avoided; and therefore FEA will consume less time; and vehicle seat manufacturer will be confident about success of the head restraint before applying the particular linear impact test and bearing the test costs.

In the following subsections, the head restraint model, the simplified seat model, positioning of the head restraint model on simplified seat model and the stiffness of the seat-back for front and rear impacts are presented.

4.1. Head Restraint Model

Computer-Aided Desing (CAD) model of the seat head restraint will be used for FEA. In the propose method, complete CAD model of head restraint is used because the study is to observe the head restraint energy absorption and observing the success of head restraint under the loading conditions during the linear impact test.

A typical head restraint can be seen in Figure 2.14. The head restraint consists of two types of foams and a connecting part referred to as the ‘armature’. Two legs of the armature are used to mount head restraint on the vehicle seat. As seen in Figure 4.1,

the outer foam has a trapezoidal shape with dimensions of 198 mm in width and 72 mm in depth at Section A-A and, 219 mm in height. The inner foam has dimensions of 141 mm in width and 45 mm in depth at Section A-A, and 140 mm in height. The armature is tube with an outer and inner diameter of 12 and 8 mm, respectively. Instead of the tube, solid bars may be used as the armature.

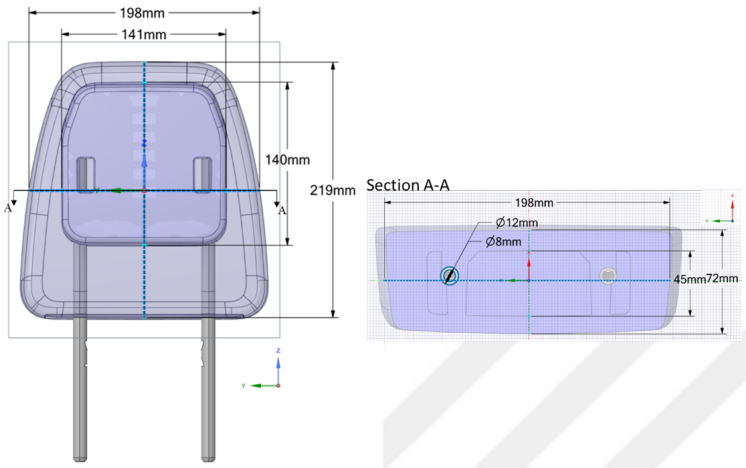

Figure 4.1. Dimensions of the head restraint

4.2. Simplified Seat Model

A bench type seat of a light commercial vehicle can be seen in Figure 2.13. CAD model of typical bench type seat is shown in Figure 4.2. The complete seat model has a complex geometry with foams, covers, structural parts, joints, seat belt parts, and some functional parts etc.

In this study, a simplified seat is modeled. The simplified seat model can be seen in Figure 4.3. The simplified seat model consists of two connected rectangular plates that are the back-plate representing the seat-back and the base-plate representing the seat-base. By this way, these two plates represent the main structure of the seat, excluding the foam and cover. The seat-base and seat-back are not perpendicular to each other, there is an angle of 5^{o} between them, similar to the original seat, as seen in Figure 4.3.

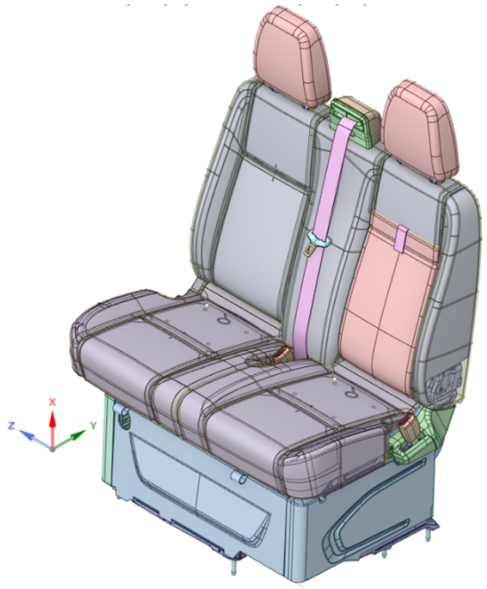

Figure 4.2. CAD model of typical bench type seat

The dimensions and mass of the simplified seat model are determined according to dimensions and mass of the seat shown in Figure 4.2. The back-plate of the simplified seat model has been adjusted to a thickness of 1.5 mm to maintain the same mass of 5.8 kg which is the mass of seat-back structure of the seat. The base-plate has the same dimensions as the seat-base of the seat. The back-plate has dimensions of 588 mm in height and 820 mm in width as seen in Figure 4.4.

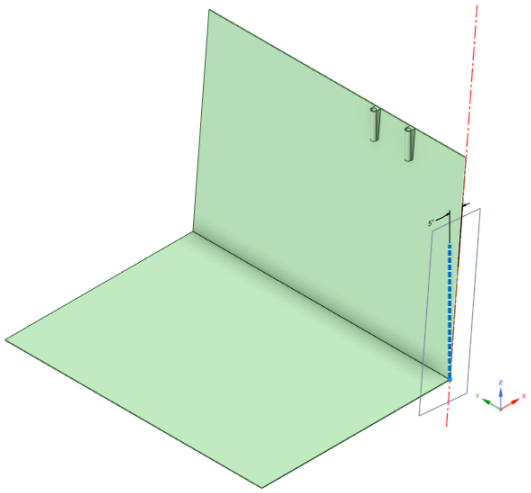

Figure 4.3. The simplified seat model

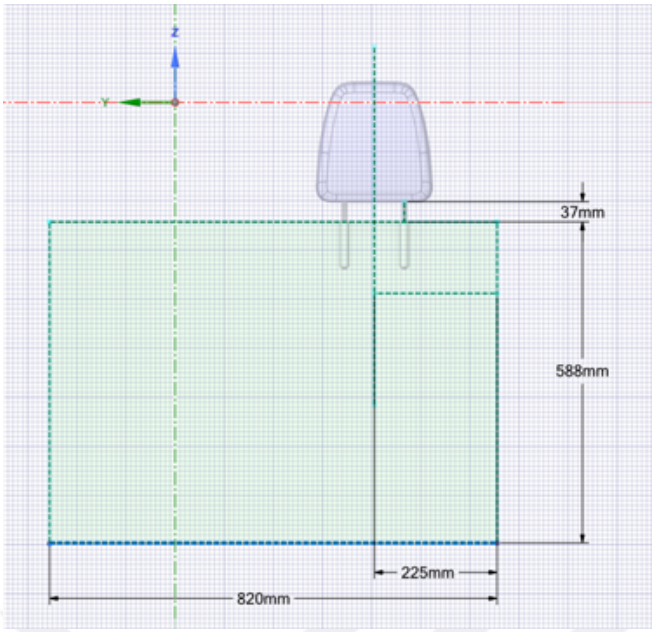

Figure 4.4. Dimensions of the simplified seat model back-plate and positioning the head restraint

4.3. Positioning Head Restraint Model on Simplified Seat Model

The relative positioning of the head restraint model on the simplified seat model is presented in Figure 4.4. The complete head restraint model on the simplified seat model is shown in Figure 4.5. The head restraint model is positioned such that the distance between the vertical axis of the head restraint and edge of the simplified seat model is 225 mm as seen in Figure 4.4. On the seat-back, two connection parts, which the legs of the armature are inserted in, are required to mount the head restraint to the seat-back. These connection parts also provide vertical alignment between the head restraint axis and z-axis as seen in Figure 4.6. Head restraint is mounted to the connection parts with a distance that in between the head restraint bottom surface and the seat-back top surface is 37 mm as seen in Figure 4.4. The seat-back is inclined at a 5^{o} angle while head restraint is parallel to the z-axis as seen in Figure 4.7.

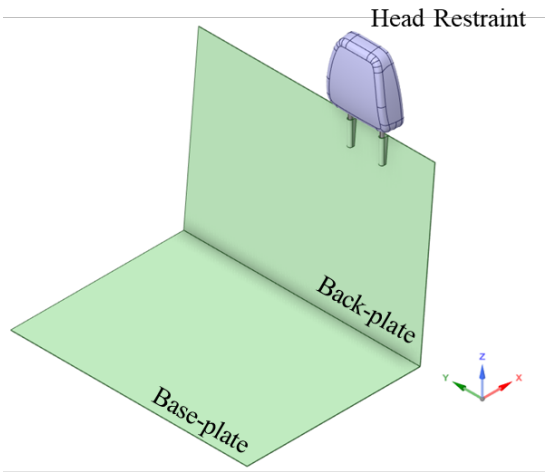

Figure 4.5. The complete head restraint model and the simplified seat model

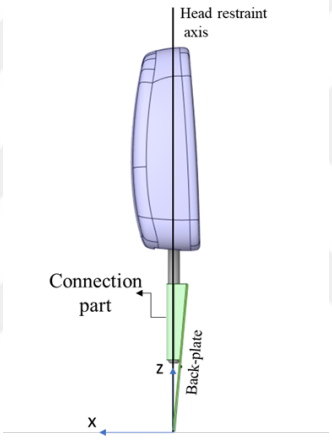

Figure 4.6. Connection Part

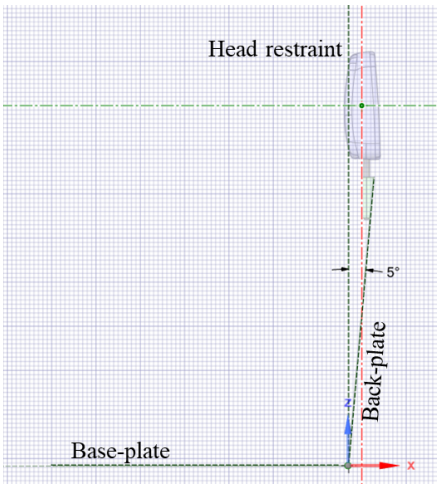

Figure 4.7. Angle between the back-plate and base-plate

4.4. Stiffness of the seat-back for front impact

In the front impact, seat-back stiffness due to resistance to clockwise direction rotation of seat-back about the joint between seat-back and seat-base components is considered. To calculate the stiffness, high-speed video recordings of the front impact test described in Chapter 2, has been examined by using an image processing software. The particular tracker on the side of the seat-back can be seen in Figure 2.20. Schematic view of the front impact test is given in Figure 4.8 for the purpose of calculation of the seat-back stiffness coefficient.

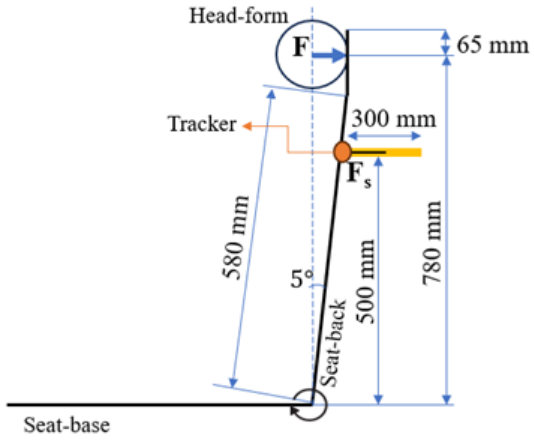

Figure 4.8. Schematic view of the front impact test for calculation of the seat-back stiffness coefficient

The seat-back stiffness coefficient at the front impact calculation is explained step by step as follows:

1. The head-form hits the head restraint at 65 mm below the top of the head restraint with the speed of 24.1 km/h and causes action force denoted by F at 780 mm above the seat-base. The reaction force of seat-back at the tracker denoted by F_s , which is parallel to seat-base, should be calculated at 500 mm above the seat-base. The relationships between them are determined based on the basic proportionality theorem in triangles as follow:

$$F(780mm) = F_s(500mm) \tag{4.1}$$

2. The force, F applied by head-form is obtained by using Newton's second law of motion formulation where m is mass and a is acceleration. For defining acceleration, the average maximum acceleration is used which is 35.4g from the experimental tests discussed in Chapter 2:

$$F = ma = (6.8kg)(35.4 \times 9.81\frac{m}{s^2}) \tag{4.2}$$

3. Substituting the result of Eq. 4.2 in Eq. 4.1:

$$[(6.8kg)(35.4 \times 9.81\frac{m}{s^2})](780mm) = F_s(500mm) \tag{4.3}$$

4. According to Eq. 4.3, F_s is calculated at the tracker as 3683.9 N.

5. Seat-back stiffness coefficient is obtained by applying Hooke's Law:

$$F_s = kx \tag{4.4}$$

6. Displacement value x is defined as 50 mm based on the images of high-speed video recorded during the experimental tests which is the maximum seat-back displacement at the tracker. Seat-back stiffness is obtained as 73.7 N/mm with substituting the force and displacement value in Eq. 4.4.

$$k = \frac{F_s}{x} = \frac{3683.9N}{50mm} = 73.7N/mm \tag{4.5}$$

This calculated stiffness value is used in the first stage of FEA study discussed in Chapter 5.

4.5. Stiffness of the seat-back for rear impact

In the rear impact, seat-back stiffness due to resistance to counter-clockwise direction rotation of seat-back about the joint between seat-back and seat-base components is considered. To calculate the stiffness, high-speed video recordings of the rear impact test described in Chapter 3, has been examined by using an image processing software. The particular tracker on the side of the seat-back can be seen in Figure 3.10. Schematic view of the rear impact test is given in Figure 4.9 for the purpose of calculation of the seat-back stiffness coefficient.

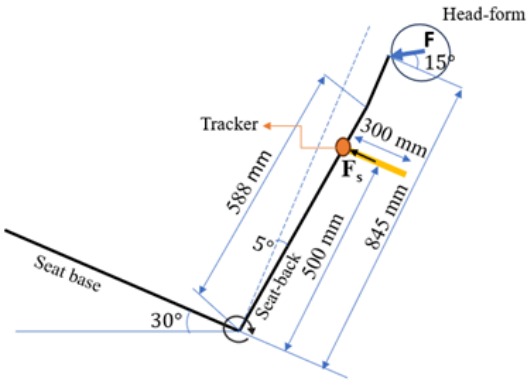

Figure 4.9. Schematic view of the rear impact test for calculation of the seat-back stiffness coefficient

The seat-back stiffness coefficient at the rear impact calculation is explained step by step as follows:

1. The head-form hits the head restraint at the top with 15^o angle from the horizontal plane as explained in Chapter 3 and causes action force denoted by F at 845 mm above the seat-base. The reaction force of seat-back at the tracker denoted by F_s , which is parallel to seat-base, should be calculated at 500 mm above the seat-base. The relationships between them are determined based on the basic proportionality theorem in triangles and considering the component of F parallel to the seat-base as follows:

$$Fcos(15)(845mm) = F_s(500mm) \tag{4.6}$$

2. The force, F applied by head-form is obtained by using Newton's second law of motion formulation where m is mass and a is acceleration. For defining acceleration, the average maximum acceleration is used which is 34.7g from the experimental tests discussed in Chapter 3:

$$F = ma = (6.8kg)(34.7 \times 9.81\frac{m}{s^2}) \tag{4.7}$$

3. Substituting the result of Eq. 4.7 in Eq. 4.6:

$$[(6.8kg)(34.7 \times 9.81\frac{m}{s^2})] \times \cos 15 \times (845mm) = F_s(500mm) \tag{4.8}$$

4. According to Eq. 4.8, F_s is calculated at the tracker as 3755.5 N.

5. Seat-back stiffness coefficient is obtained by applying Hooke's Law:

$$F_s = kx \tag{4.9}$$

6. Displacement value x is defined as 15 mm based on the images of high-speed video recorded during the experimental tests which is the maximum seat-back displacement at the tracker. Seat-back stiffness is obtained as 250 N/mm with substituting the force and displacement value in Eq. 4.10.

$$k = \frac{F_s}{x} = \frac{3755.5N}{15mm} = 250N/mm \tag{4.10}$$

This calculated stiffness value is used in the first stage of FEA study discussed in Chapter 6.

CHAPTER 5

FINITE ELEMENT ANALYSIS OF THE HEAD RESTRAINT WITH THE SIMPLIFIED SEAT MODEL FOR THE FRONT IMPACT

Compared to physical tests, computer simulations save time and cost, and provide tools to study variable conditions and geometries, thus simulations are widely preferred during development process in automotive industry. Finite element analysis (FEA) is the most used method for designing and developing components and structures of vehicles in the automotive industry. Computer simulations are generally used to realize the response of occupant and restraint systems such as seat, head restraint in collision [40], [49],[50].

Some of FEA software are specialized for crashworthiness such as LS-DYNA [51], PAM-CRASH [52], MADYMO [34] etc. Every software package has its own advantages and disadvantages. According to review done by Zhang et al. [53], if rapid model setup and runtime are considered, MADYMO is advisable; and PAM-CRASH can be preferred if kinematics is significant [54].

LS-DYNA is widely common FEA software and it provides maximum user control over the model and solves explicit dynamic problems [51]. LS-DYNA was developed by Livermore Software Technology Corporation (LSTC) in 1988, then in 2019, it was purchased by ANSYS. ANSYS LS-DYNA is also preferred because of simplicity of the user interface.

In this chapter, Finite Element Model (FEM) and Finite Element Analysis of the head restraint with the simplified seat model for the front impact are introduced and the impact loading is simulated according to Annex 6 of UN ECE R17 [18]. ANSYS LS-DYNA software has been used for preparing, solving and post-processing [51].

5.1. Finite Element Modelling of The Head Restraint with Simplified Seat Model for The Front Impact

According to the Annex 6 of UN ECE R17 regulation, the front impact test simulations are performed by impacting the head-from with the mass of 6.8 kg and the diameter of 165 mm to the head restraint as experimentally applied which has been explained in Chapter 2. In the FEM, the head-form is created as a sphere with the diameter of 165 mm by using the ANSYS SpaceClaim 3D Modelling Software [55] as seen in Figure 5.1. The material of the head-form is defined as aluminium which is the same with the head-form (i.e. impactor) used in METU-BILTIR Center Vehicle Safety Unit.

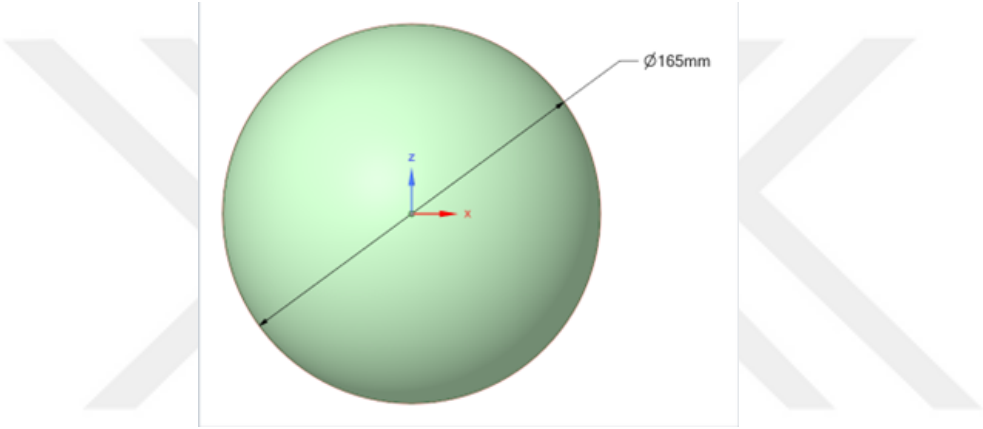

Figure 5.1. FEM of the head-form

As seen in Figure 5.2, the front impact is simulated with hitting the front side of the head restraint by the head-form. The head-form is positioned at 65 mm below the top of the head restraint and touches to the front surface of the head restraint. The head restraint with the simplified seat model has been given in Figure 4.5 and Figure 4.6.

Description of materials, mesh definition, contact types and constraints used in this study are given in the following sub-sections.

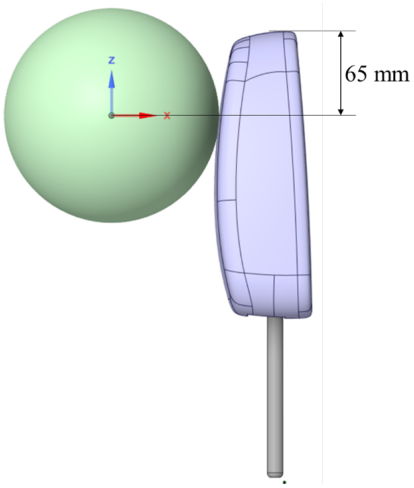

Figure 5.2. Head-form position for front impact FEM

5.1.1. Description of Materials

A typical seat is made up of head restraint, seat-back, seat-base and some functional parts. For occupant safety, materials of head restraint, seat-back and seat-base are important and, foams are used because of their highly energy consumption capabilities. However, modelling of these materials is complex and obtaining the dynamic behavior of foams is highly difficult in computer simulation [50]. Since LS-DYNA library contains wide range of material cards for foams, LS-DYNA material cards are used for proper definition of foam material specifications in this study. Material card should be chosen according to expected behavior of material during impact [56, 57] and correct material parameters should be input to the software.

Polyurethane (PU) and Expanded Polypropylene (EPP) foams are mostly used materials in crashworthiness of vehicles [58]. In this study, the foam components of the head restraint are combination of two different foams with same density of 40 kg/m^3 according to information obtained from the manufacturer of the particular seat and head restraint. The inner foam is specified as EPP and the outer foam is Polyurethane. LS-DYNA MAT 057 Low Density Foam material card is used.

MAT 057 Low Density Foam material card is preferred for low-density, highly compressible and recoverable foams which are used in seat cushion, padding, side impact etc. [59]. For definition, it needs density, Young's modulus, nominal stress-strain

curve. For recovery behavior, hysteric unloading factor and shape factor are considered [60, 61]. Young's modulus and Poisson's ratio values do not affect the material behavior of compression condition in MAT 057 material card. Because MAT 057 material card uses Young's modulus for described tension and it has no formulation that includes Poisson's ratio [62]. It is hard to obtain the specific foam material properties such as poisons ratio and rate dependent nominal stress-strain curve, therefore Mat 057 card which can be defined with the available material data is preferred. This material card is used both foams. The used material properties are given below:

Density = 40 kg/m^3

Young's Modulus = 10 MPa

Nominal stress-strain curve is given in Figure 5.3.

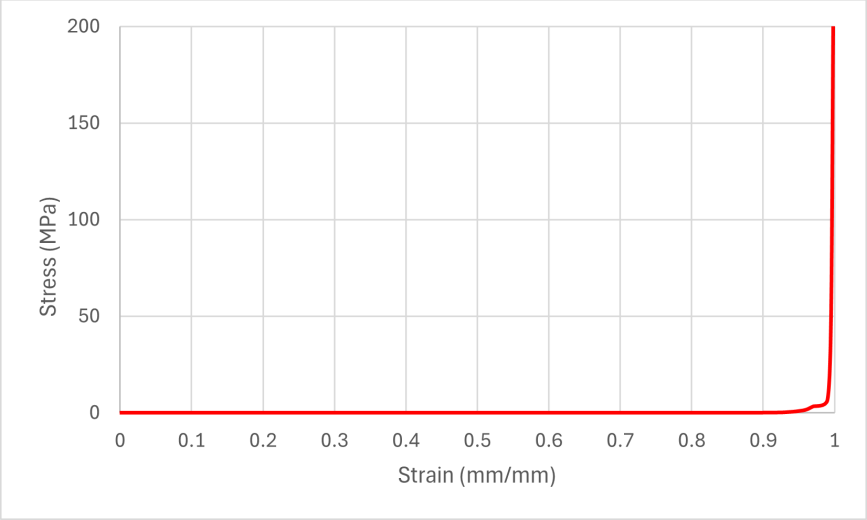

Figure 5.3. Nominal stress versus strain curve for foams

Metallic parts of the simplified seat and the head restraint are defined with LS-DYNA material cards which are MAT 001 Elastic, MAT 020 Rigid and MAT 024 Piecewise Linear Plasticity as explained in the following paragraphs.

Seat-back and seat-base of the simplified seat model are defined as structural steel and MAT 001 Elastic card is used. This material card is used for isotropic elastic materials. Head-form is defined as aluminium and MAT 020 Rigid Material Card is used. This material card is used for modelling rigid bodies. Both cards density, Young's modulus and Poisson's ratio are needed [61]. Deformation of the seat-back

and seat-base are not in the scope of this study, therefore MAT 001 Elastic card which requires limited number of material properties is preferred to define structural steel. Likewise, head-form material which is aluminium is defined with MAT 020 because it is considered as rigid part and its deformation is neglected. Material parameters for aluminium and structural steel are given in Table 5.1.

Table 5.1. Material parameters for aluminium and structural steel

Material	Density kg/m^3	Young's Modulus (GPa)	Poisson's Ratio
Aluminium	2850	70	0.33
Structural Steel	7850	210	0.3

The armature in the head restraint is defined as ST52 Steel and MAT 024 Piecewise Linear Plasticity Material Card is used for it. This material card is an elasto-plastic material and strain rate dependent stress versus strain curve can be defined. Several studies have revealed that if the material is subjected to large impact, strain rate dependent parameters should be considered for more realistic results. One of the most common material models is Cowper Symonds and its formulation is used for the strain rate effects. For a definition of this card, density, Young's modulus, Poisson's ratio, yield stress, load curve and, if the strain rate effect is considered, tangent modulus and along with strain rate parameters C and p are required [61, 63]. Strain rate parameters C and p are taken from the study of Skrlec and Klemenc [63]. Stress versus strain curve is given by the manufacturer. Material parameters for ST52 Steel are given below.

Density = 7850 kg/m^3

Young's Modulus = 210 GPa

Poisson's Ratio = 0.3

Yield Stress = 460.8 MPa

Tangent Modulus = 0.955 GPa

Strain Rate Parameter C = 41.013 ms^{-1}

Strain Rate Parameter p = 6.2

Stress versus strain curve for ST52 Steel is given in Figure 5.4.

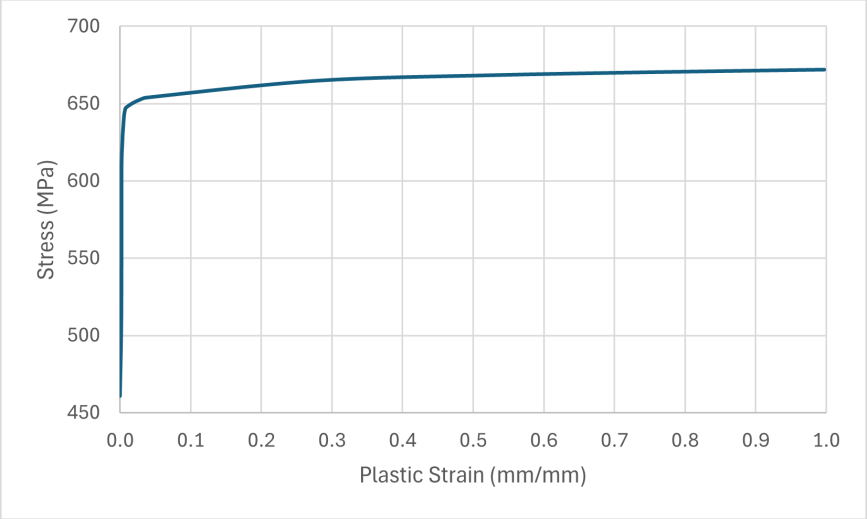

Figure 5.4. Stress versus strain curve for ST52 Steel

The summary of materials and material cards is given in Table 5.2

Table 5.2. Summary of used materials and material cards

Part Name	Material	Material Card
Foams	Polyurethane-EPP	MAT 057
Armature	ST52 Steel	MAT 024
Head-form	Aluminium	MAT 020
Seat-back	Structural Steel	MAT 001
Seat-base	Structural Steel	MAT 001

5.1.2. Definition of Mesh

Tetrahedron element type uses triangular shape elements which makes it quicker to apply meshes and also geometry with holes or curvature can be easily meshed. However, it increases solver time since mesh cannot be smooth. On the other hand, hexahedron element type uses square shape elements which provides smoother mesh and reduced solver time [64]. Despite these advantages, applying hexahedron elements requires more optimization time.

The tetrahedron and hexahedron elements are used for meshing of different components in this study. According to the concerns described above, the mesh is generated with the tetrahedron elements for the seat-back, foams and armature of the head restraint. The hexahedron elements are used for the head-form and the seat-base. In the model, there are 38857 tetrahedron and 2993 hexahedron elements which makes in total of 41850 elements. The model with the tetrahedron and hexahedron elements is shown in Figure 5.5.

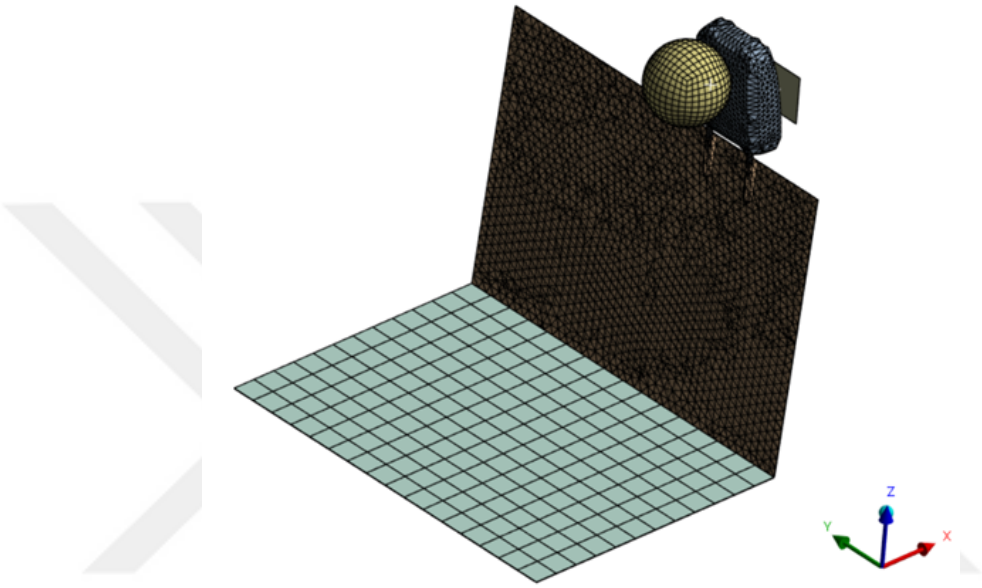

Figure 5.5. The model with tetrahedron and hexahedron elements

5.1.3. Contacts and Constraints

Two different contact types have been used in the model as “bonded contact” and “frictional contact”. The head restraint components have been explained in Chapter 4. “Bonded contact” is applied between inner and outer foams of the head restraint and between these foams of the head restraint and armature. In LS-DYNA, this contact type is called as “Tied_Surface_To_Surface_Offset” and it is recommended to be used for surfaces which are very close to each other and which do not have relative motion with respect to each other [65]. “Frictional contact” is called as "Automatic_Single_Surface"in LS-DYNA. “Frictional contact” is defined between the head-form and head restraint. The friction coefficient is given as 0.1 based on the similar study of Laban [40].

In FEM, a revolute joint and a spring are added for simulating reclining of the seat-back as seen in Figure 5.6 and Figure 5.7. The revolute joint is defined in between the bottom edge of the seat-back and rear edge of the seat-base. The revolute joint provides reclining of the seat-back. The seat-back contributes to the absorption of the impact energy by reclining. The reclining limit is defined with the spring parameters. The "longitudinal spring" is added to the simplified seat model together with spring stiffness and damping coefficients. Spring is created between the rear side of the seat-back and the spring base-plate which is a vertical fictitious plane as seen in Figure 5.6. The distance between the seat-back and the spring base-plate (i.e. between point-A and point-B) is defined as 300 mm as seen Figure 5.7. The distance between point-B and point-G is 500 mm as seen in Figure 5.7. The spring base-plate is meshed with the hexahedron elements.

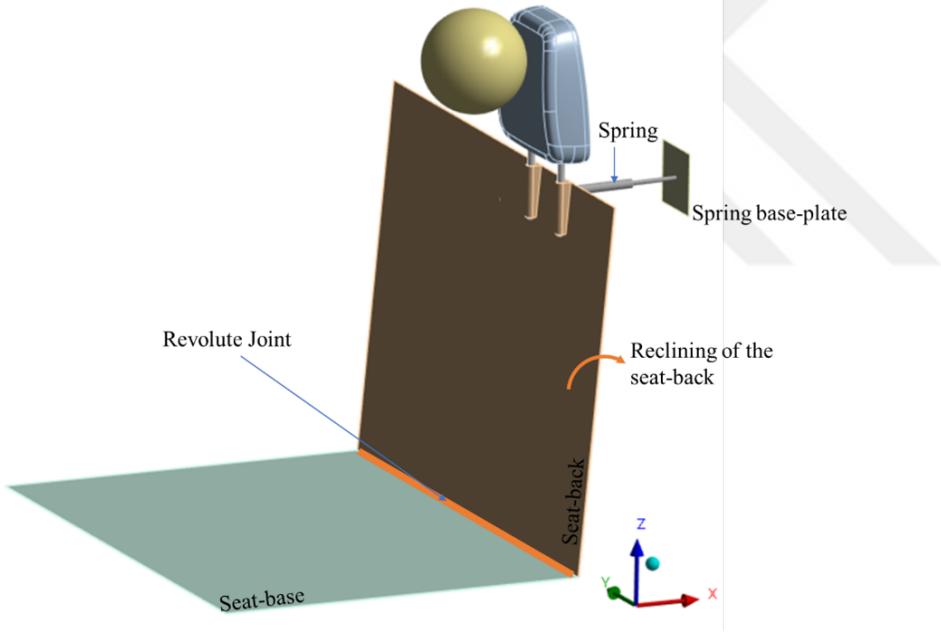

Figure 5.6. The simplified seat model with spring and revolute joint

The seat-base is fixed in all directions at the surface and likewise, the spring base-plate is fixed in all directions at the surface. They are defined in LS-DYNA with "rigid body constrained". Then, the head-form is restricted in all directions except the impact direction which is x-axis as seen Figure 5.8 since the guided head-form is used which is free to move only in impact direction.

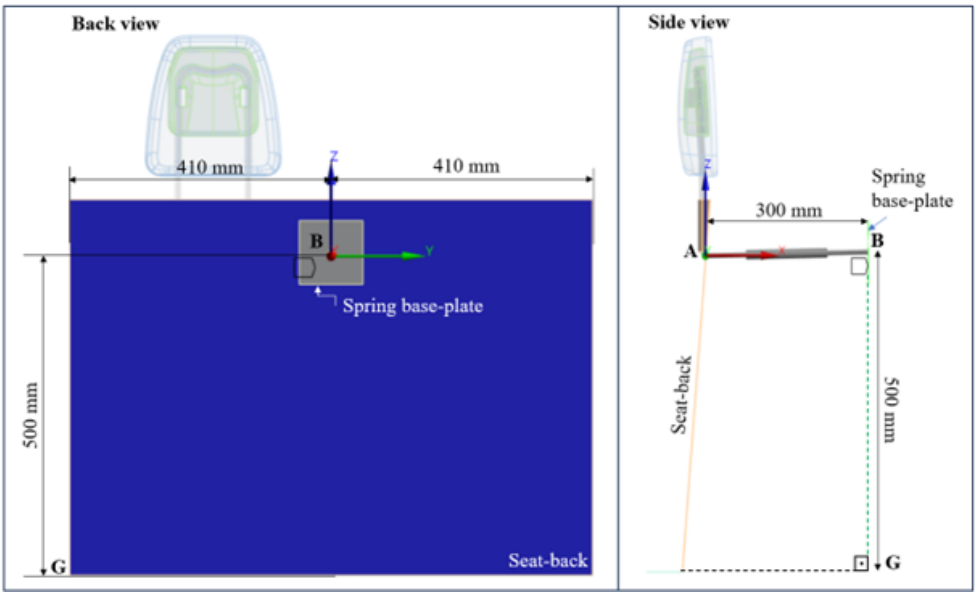

Figure 5.7. The spring in FEM

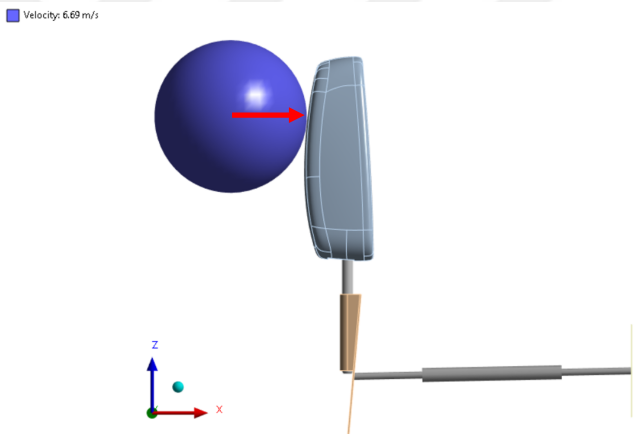

Figure 5.8. Impact direction in front impact FEM

5.2. Finite Element Analysis of The Head Restraint with Simplified Seat Model for The Front Impact

After FEM has been completed as described in Section 5.1, several FEA attempts for the front impact of the head restraint have been done by using different parameter values. In all simulations, the impact speed is applied as 6.69 m/s (24.1 km/h) as defined in the regulation [18].

In the following sub-sections, FEA studies with different spring stiffness coefficients and different damping coefficients will be presented. FEA results are compared with the experimental tests results and the regulation requirements [18].

5.2.1. FEA Studies with Different Spring Stiffness Coefficients

As discussed in Section 5.1 , a revolute joint and a spring are added for simulating reclining of the seat-back in FEM. Spring stiffness and damping coefficients are given to LS-DYNA FEM. The stiffness of the seat-back is calculated as 73.7 N/mm depending on the experimental tests results as discussed in Section 4.4. However, FEA has been realized for the spring stiffness coefficients of 50 N/mm, 73.7 N/mm, 100 N/mm, 150 N/mm, 250 N/mm, 350 N/mm, and 500 N/mm to see the effect of the spring stiffness coefficient on FEA results. Damping coefficient is given as 0.2 Ns/mm for these simulations. The acceleration versus time curves are shown in Figure 5.9-5.14 and the maximum acceleration values are tabulated in Table 5.3.

a. FEA with spring stiffness coefficient of 50 N/mm: The acceleration versus time curve is given Figure 5.9 and the maximum acceleration of the head-form is 31.5g.

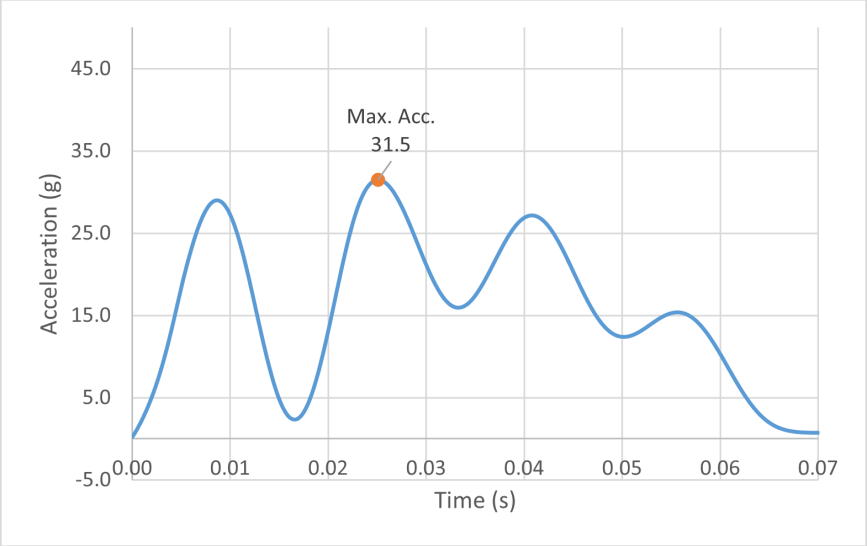

Figure 5.9. Acceleration versus time curve of spring stiffness coefficient 50 N/mm with damping coefficient 0.2 Ns/mm in front impact

b. FEA with spring stiffness coefficient of 73.7 N/mm: The acceleration versus time curve is given Figure 5.10 and the maximum acceleration of the head-form is 34.0g.

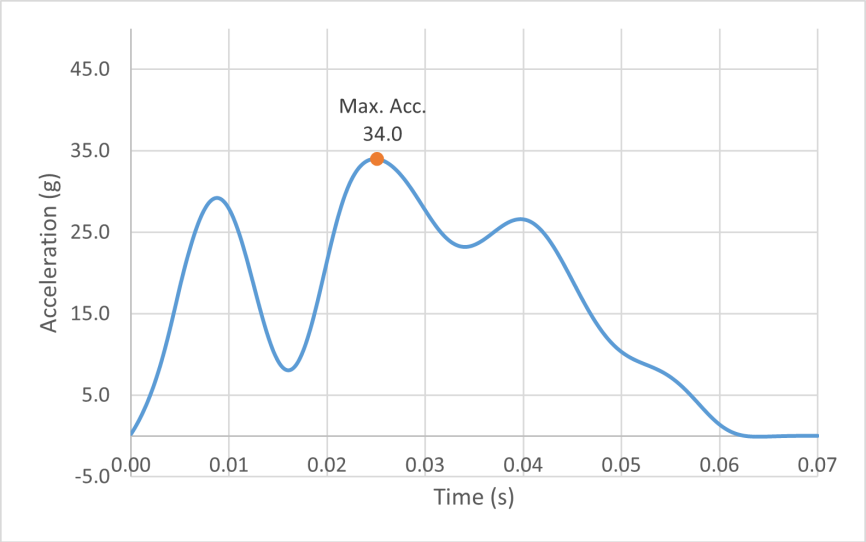

Figure 5.10. Acceleration versus time curve of spring stiffness coefficient 73.7 N/mm with damping coefficient 0.2 Ns/mm in front impact

c. FEA with spring stiffness coefficient of 100 N/mm: The acceleration versus time curve is given Figure 5.11 and the maximum acceleration of the head-form is 36.1g.

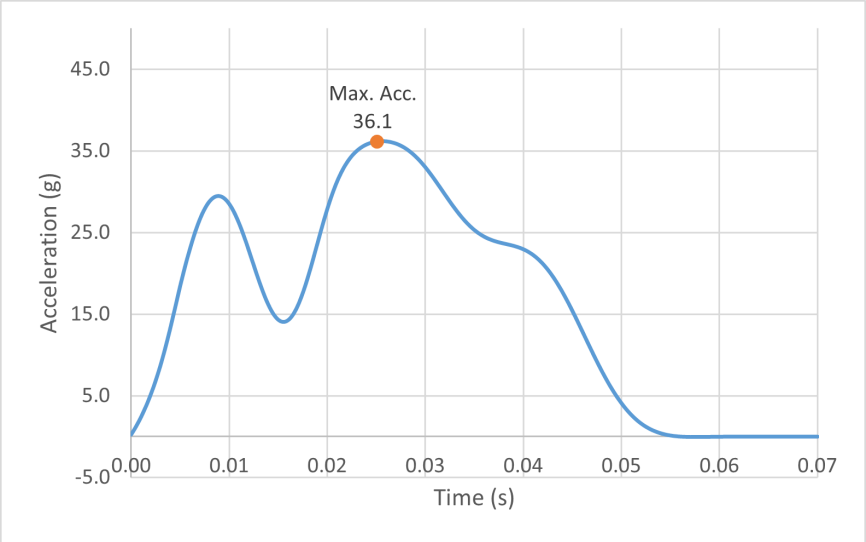

Figure 5.11. Acceleration versus time curve of spring stiffness coefficient 100 N/mm with damping coefficient 0.2 Ns/mm in front impact

d. FEA with spring stiffness coefficient of 150 N/mm: The acceleration versus time curve is given Figure 5.12 and the maximum acceleration of the head-form is 39.6g.

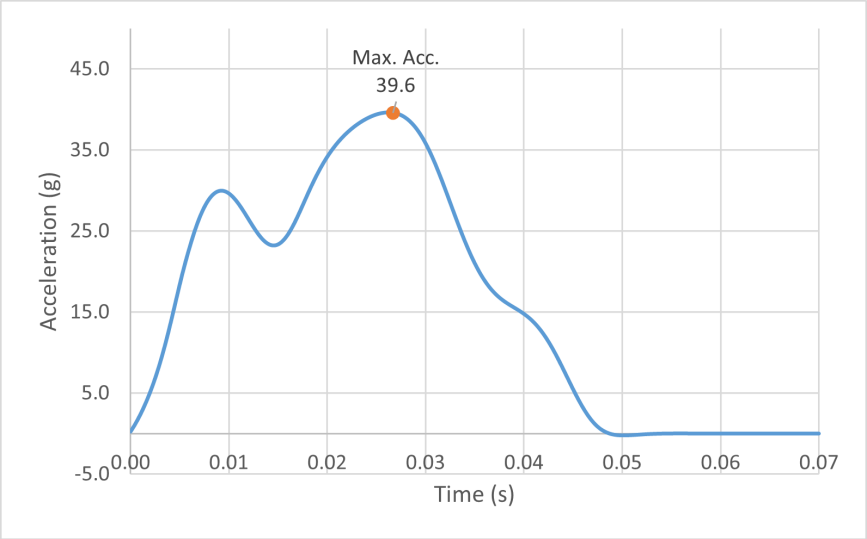

Figure 5.12. Acceleration versus time curve of spring stiffness coefficient 150 N/mm with damping coefficient 0.2 Ns/mm in front impact

e. FEA with spring stiffness coefficient of 250 N/mm: The acceleration versus time curve is given Figure 5.13 and the maximum acceleration of the head-form is 43.4g.

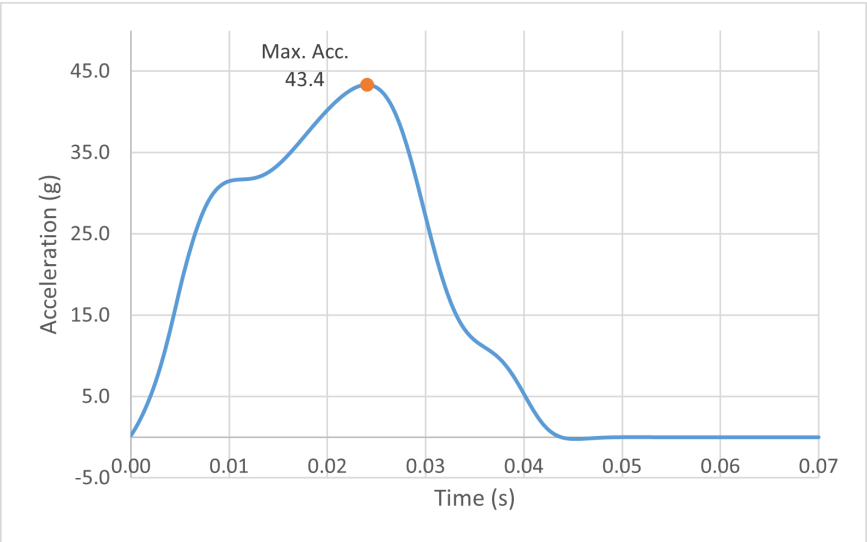

Figure 5.13. Acceleration versus time curve of spring stiffness coefficient 250 N/mm with damping coefficient 0.2 Ns/mm in front impact

f. FEA with spring stiffness coefficient of 500 N/mm: The acceleration versus time curve is given Figure 5.14 and the maximum acceleration of the head-form is 45.7g.

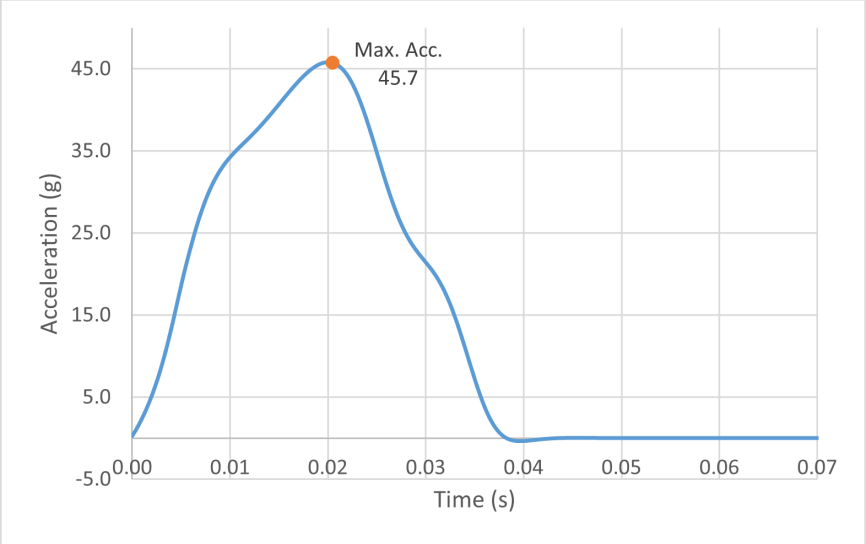

Figure 5.14. Acceleration versus time curve of spring stiffness coefficient 500 N/mm with damping coefficient 0.2 Ns/mm in front impact

As given in Table 2.1, the experimental acceleration results are 37.0g, 34.7g, 34.5g for three front impact tests and the average acceleration is calculated as 35.4g. In FEA, the maximum acceleration is found as 34.0g for the spring stiffness coefficient of 73.7 N/mm. This FEA result is in correlation with the experimental result within the acceptable range.

Table 5.3. The maximum acceleration values found for different spring stiffness coefficient values for the front impact

Spring Stiffness Coefficient	Maximum Acceleration
50 N/mm	31.5g
73.7 N/mm	34.0g
100 N/mm	36.1g
150 N/mm	39.6g
250 N/mm	43.4g
500 N/mm	45.7g

As it is seen in Table 5.3, the maximum acceleration values increases when spring stiffness coefficient (in the range of 50-500 N/mm) increases. Additionally, as seen in the acceleration versus time curves (Figure 5.9-5.14) and Table 5.3, the maximum

acceleration values are below 80g, therefore these values satisfy the regulation [18]. Even for high spring stiffness coefficient such as 500 N/mm, FEA result shows that the maximum acceleration value (45.7g) is quite below 80g. Therefore, the proposed method in this study which includes the constructed FEM with the simplified seat model and FEA of the front impact test can be used by head restraint manufacturers to have an idea for the energy absorbing performance of their product before conduction linear impact tests according to Annex 6 of UN ECE R17.

5.2.2. FEA Studies with Different Damping Coefficients

FEA simulations have been repeated for the damping coefficient of 0 Ns/mm, 0.1 Ns/mm, and 0.2 Ns/mm to see effect of the damping coefficient on FEA results. The spring stiffness coefficient is input as 73.7 N/mm for these simulations. The acceleration versus time curves are shown in Figure 5.15-5.17 and the maximum acceleration values are tabulated in Table 5.4.

a. FEA with damping coefficient of 0 Ns/mm: The acceleration versus time curve is given Figure 5.15 and the maximum acceleration of the head-form is 33.8g.

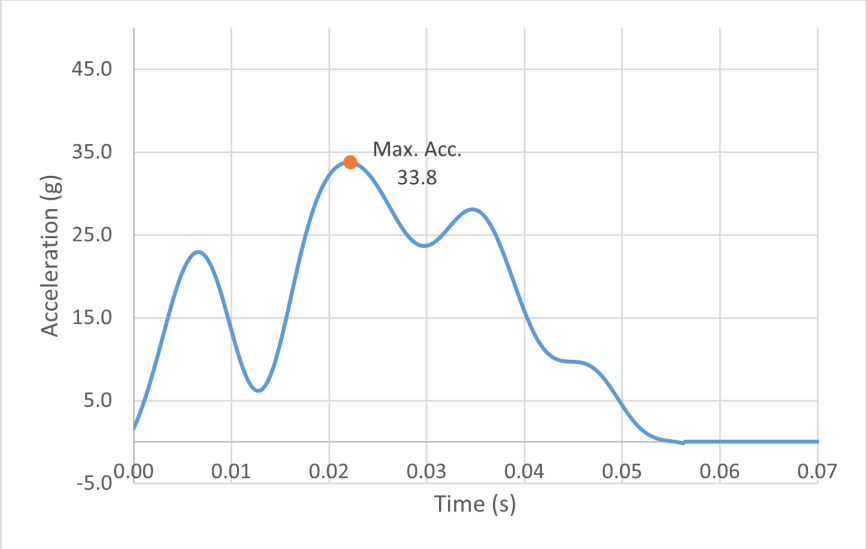

Figure 5.15. Acceleration versus time curve of damping coefficient 0 Ns/mm with spring stiffness coefficient 73.7 N/mm in front impact

b. FEA with damping coefficient of 0.1 Ns/mm: The acceleration versus time curve is given Figure 5.16 and the maximum acceleration of the head-form is 33.9g.

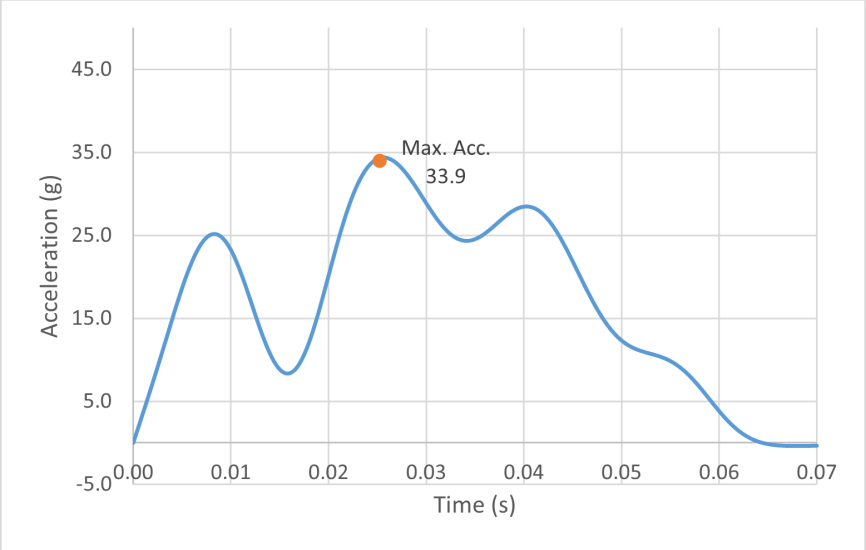

Figure 5.16. Acceleration versus time curve of damping coefficient 0.1 Ns/mm with spring stiffness coefficient 73.7 N/mm in front impact

c. FEA with damping coefficient of 0.2 Ns/mm: The acceleration versus time curve is given Figure 5.17 and the maximum acceleration of the head-form is 34.0g.

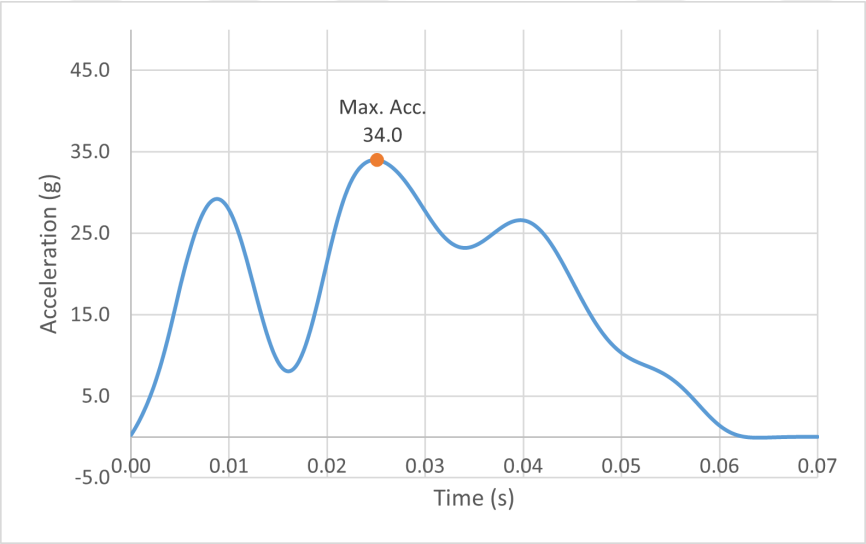

Figure 5.17. Acceleration versus time curve of damping coefficient 0.2 Ns/mm with spring stiffness coefficient 73.7 N/mm in front impact

Table 5.4. The maximum acceleration values found for different damping coefficient values for the front impact

Damping Coefficient	Maximum Acceleration
0 Ns/mm	33.8g
0.1 Ns/mm	33.9g
0.2 Ns/mm	34.0g

As it is seen in Table 5.4 the maximum acceleration values are not affected significantly when damping coefficient (in the range of 0-0.2 Ns/mm) is changed for the same spring stiffness coefficient.

CHAPTER 6

FINITE ELEMENT ANALYSIS OF HEAD RESTRAINT WITH SIMPLIFIED SEAT MODEL FOR REAR IMPACT

In this chapter, Finite Element Model (FEM) and Finite Element Analysis (FEA) of the head restraint with the simplified seat model for the rear impact are presented. In FEA, impact simulation is performed according to Annex 6 of UN ECE R17 [18].

6.1. Finite Element Modelling of the Head Restraint with the Simplified Seat Model for the Rear Impact

FEM for the rear impact is very similar with FEM for the front impact. However, there are some differences especially relative positioning of the head restraint and the head-form. The rear impact is simulated with hitting the back-top of the head restraint by the head-form. FEM represents experimental test model. The simplified seat model is rotated 30^{o} relative to horizontal axis as seen in Figure 6.1 The angle in between center of the head-form and the top point of the head restraint is 15^{o} as seen in Figure 6.2 The head-form touches to the top point of the head restraint. Description of materials, mesh definition and contact types are the same with the front impact model and detail of the definition is given in Section 5.1. The constraints are also defined similar to the front impact model. Head-form is restricted in all directions except the impact direction which is x'-axis shown in Figure 6.2.

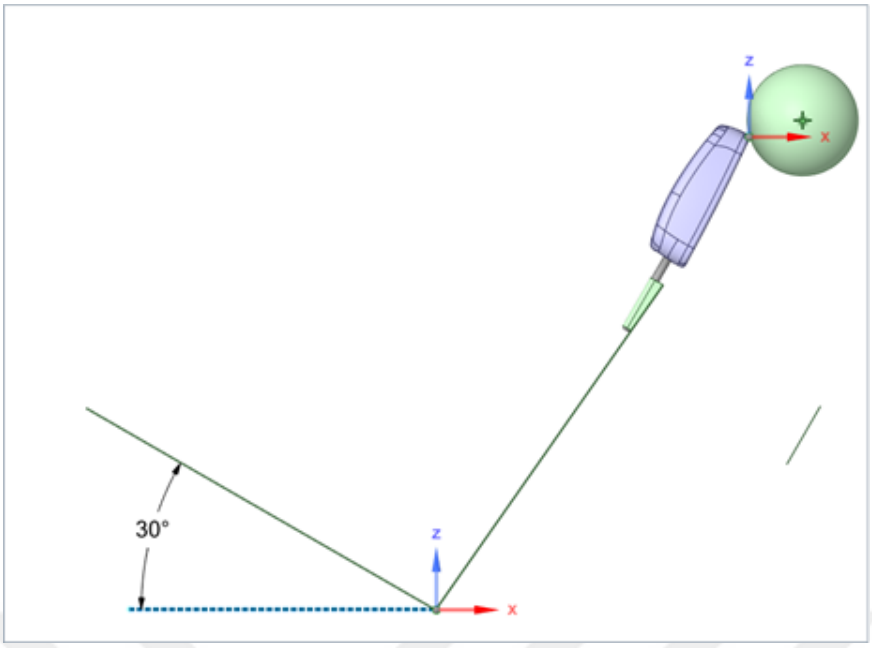

Figure 6.1. Simplified seat position for rear impact FEM

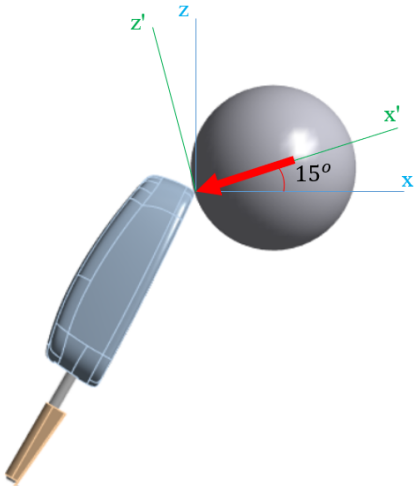

Figure 6.2. Impact direction in rear impact FEM

6.2. Finite Element Analysis of The Head Restraint with Simplified Seat Model for The Rear Impact

After FEM has been completed, several FEA attempts for the rear impact have been done similar to the front impact by using different parameter values. In all simulations, the impact speed is applied as 6.69 m/s (24.1 km/h) as defined in the regulation [18].

In the following sub-sections, FEA studies with different spring stiffness coefficients and different damping coefficients will be presented. FEA results are compared with the experimental tests results and the regulation requirements.

6.2.1. FEA Studies with Different Spring Stiffness Coefficients

The stiffness of the seat-back has been calculated as 250 N/mm depending on the experimental tests results as discussed in Section 4.5. However, FEA has been realized for the spring stiffness coefficient of 50 N/mm, 150 N/mm, 250 N/mm, 350 N/mm and 500 N/mm to see the effect of the spring stiffness coefficient on FEA results. The damping coefficient is given as 0.2 Ns/mm for these simulations. The acceleration versus time curves are shown in Figure 6.3-6.7 and the maximum acceleration values are tabulated in Table 6.1.

a. FEA with spring stiffness coefficient of 50 N/mm: The acceleration versus time curve is given in Figure 6.3 and the maximum acceleration of the head-form is 37.8g.

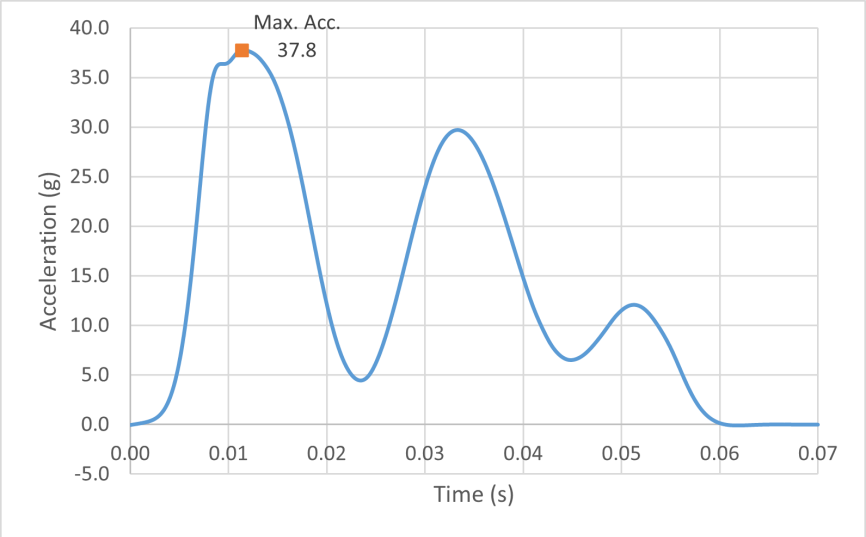

Figure 6.3. Acceleration versus time curve of spring stiffness coefficient 50 N/mm with damping coefficient 0.2 Ns/mm in rear impact

b. FEA with spring stiffness coefficient of 150 N/mm: The acceleration versus time curve is given in Figure 6.4 and the maximum acceleration of the head-form is 37.5g.

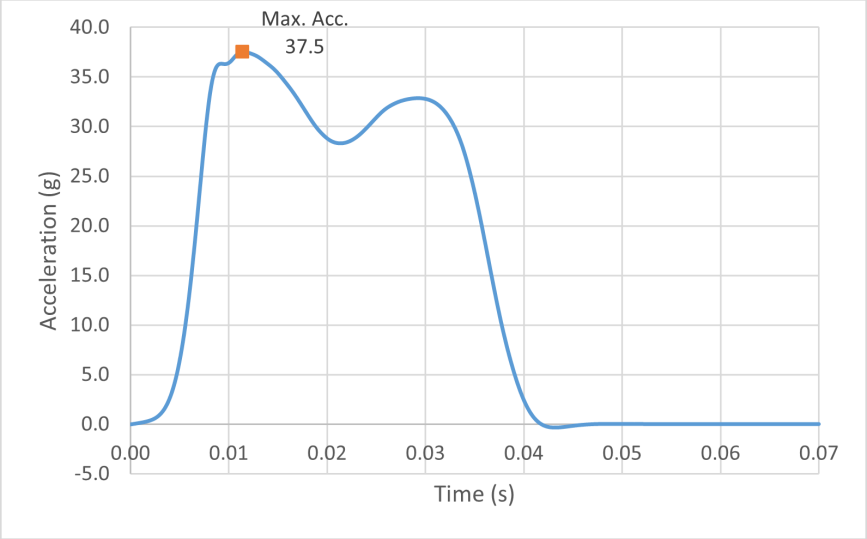

Figure 6.4. Acceleration versus time curve of spring stiffness coefficient 150 N/mm with damping coefficient 0.2 Ns/mm in rear impact

c. FEA with spring stiffness coefficient of 250 N/mm: The acceleration versus time curve is given in Figure 6.5 and the maximum acceleration of the head-form is 37.5g.

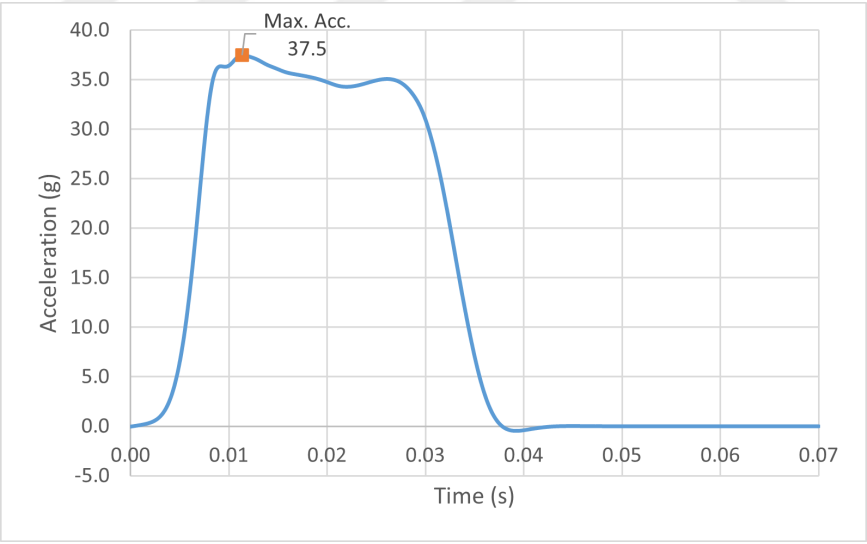

Figure 6.5. Acceleration versus time curve of spring stiffness coefficient 250 N/mm with damping coefficient 0.2 Ns/mm in rear impact

d. FEA with spring stiffness coefficient of 350 N/mm: The acceleration versus time curve is given in Figure 6.6 and the maximum acceleration of the head-form is 37.6g.

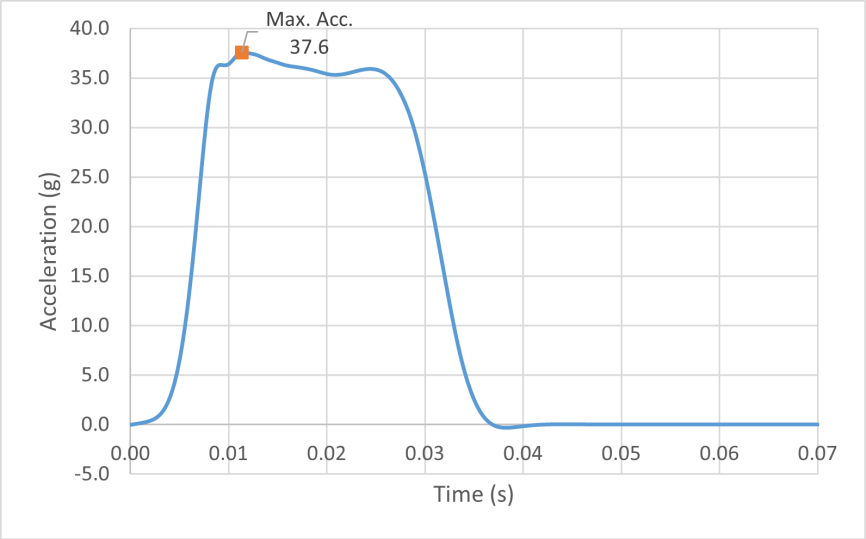

Figure 6.6. Acceleration versus time curve of spring stiffness coefficient 350 N/mm with damping coefficient 0.2 Ns/mm in rear impact

e. FEA with spring stiffness coefficient of 500 N/mm: The acceleration versus time curve is given in Figure 6.7 and the maximum acceleration of the head-form is 37.6g.

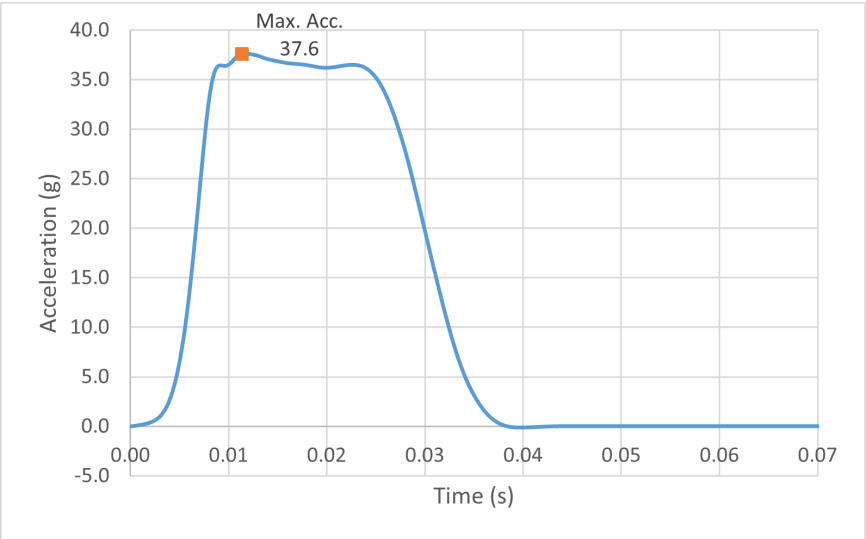

Figure 6.7. Acceleration versus time curve of spring stiffness coefficient 500 N/mm with damping coefficient 0.2 Ns/mm in rear impact

As given in Table 3.1, the experimental acceleration results are 35.4g, 33.6g, 35.1g for three rear impact tests and the average acceleration is calculated as 34.7g. In FEA, the maximum acceleration is found as 37.5g for the spring stiffness coefficient of 250 N/mm. This FEA result has validated is in correlation with the experimental result within the acceptable range.

Table 6.1. The maximum acceleration values found for different spring stiffness coefficients values for the rear impact

Spring Stiffness Coefficient	Maximum Acceleration
50 N/mm	37.8g
150 N/mm	37.5g
250 N/mm	37.5g
350 N/mm	37.6g
500 N/mm	37.6g

As it is seen in Table 6.1 the maximum acceleration values are not affected significantly when spring stiffness coefficient (in the range of 50-500 N/mm) increases. As seen in the acceleration versus time curves (Figure 6.3-6.7) and Table 6.1, the maximum acceleration values are below 80g, therefore these values satisfy the regulation [18]. Therefore, the proposed method which includes the constructed FEM with the simplified seat model and FEA of the rear impact test can be used by head restraint manufacturers to have an idea for the energy dissipation performance of their product.

6.2.2. FEA Studies with Different Damping Coefficients

FEA studies have been repeated for the damping coefficient of 0 Ns/mm, 0.1 Ns/mm and 0.2 Ns/mm. The acceleration versus time curves are shown in Figure 6.8-6.10 and the maximum acceleration values are given in Table 6.2.

a. FEA with damping coefficient of 0 Ns/mm: The acceleration versus time curve is given in Figure 6.8 and the maximum acceleration of the head-form is 37.4g.

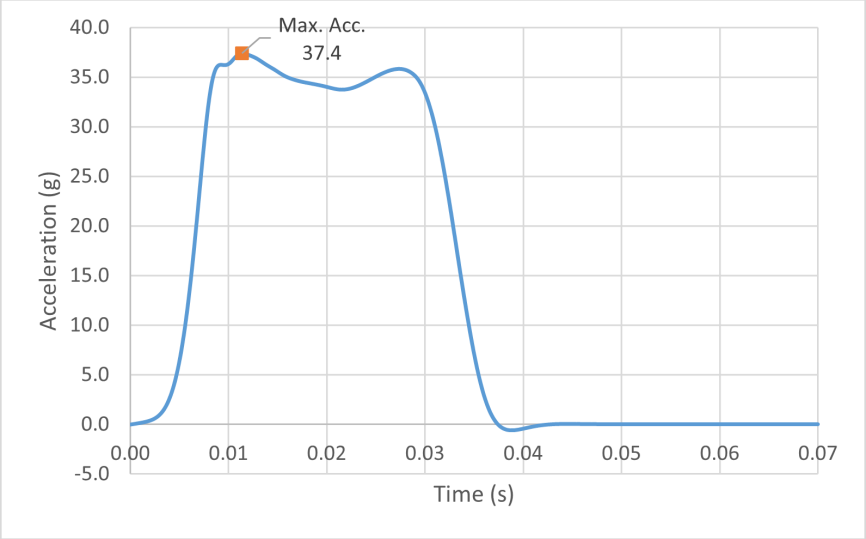

Figure 6.8. Acceleration versus time curve of damping coefficient 0 Ns/mm with spring stiffness coefficient 250 N/mm in rear impact

b. FEA with damping coefficient of 0.1 Ns/mm: The acceleration versus time curve is given in Figure 6.9 and the maximum acceleration of the head-form is 37.5g.

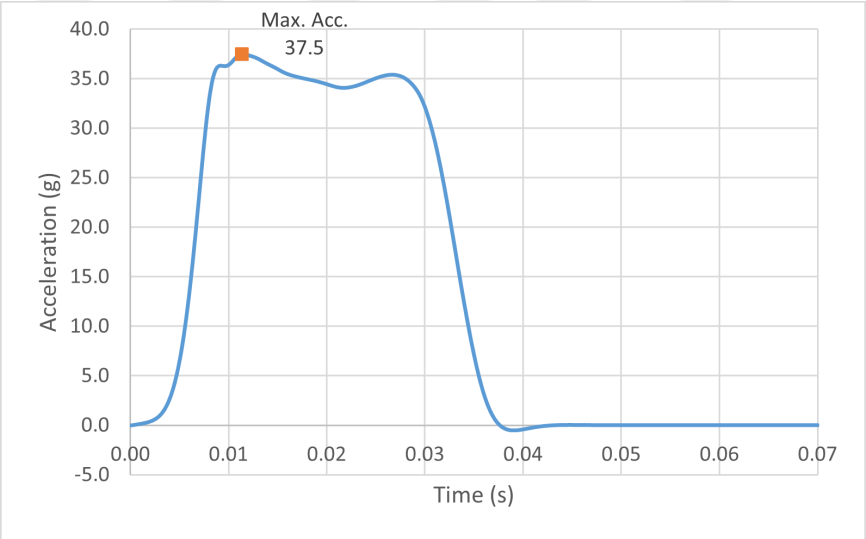

Figure 6.9. Acceleration versus time curve of damping coefficient 0.1 Ns/mm with spring stiffness coefficient 250 N/mm in rear impact

c. FEA with damping coefficient of 0.2 Ns/mm: The acceleration versus time curve is given in Figure 6.10 and the maximum acceleration of the head-form is 37.5g.

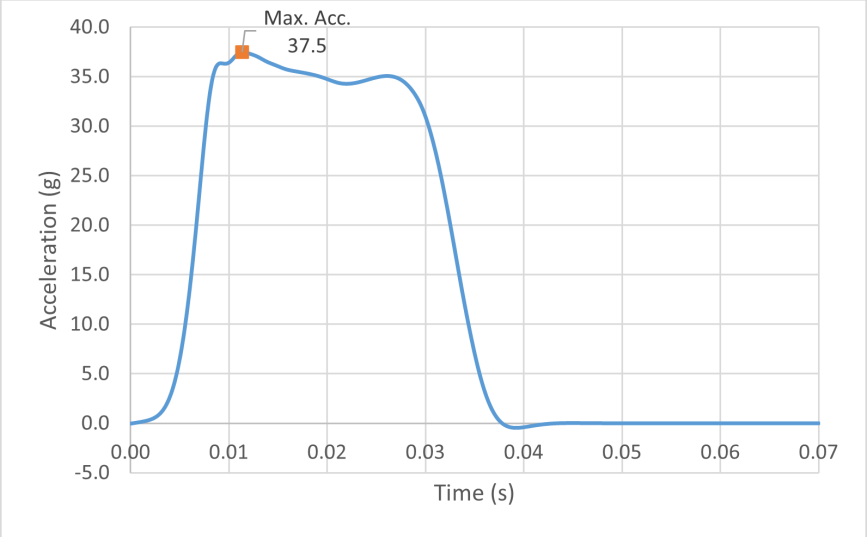

Figure 6.10. Acceleration versus time curve of damping coefficient 0.2 Ns/mm with spring stiffness coefficient 250 N/mm in rear impact

Table 6.2. The maximum acceleration values found for different damping coefficients values for the rear impact

Damping Coefficient	Maximum Acceleration
0 Ns/mm	37.4g
0.1 Ns/mm	37.5g
0.2 Ns/mm	37.5g

As it is seen in Table 6.2, it can be said that there is no significant effect of the damping coefficient (in the range of 0-0.2 Ns/mm) on the maximum acceleration of head-form.

CHAPTER 7

CONCLUSION

7.1. General Conclusions

The following conclusions of the thesis study can be summarized as follows:

- Preparation, performing and post-test activities for the front and rear impact tests on the linear impact test system have been described in detail.
- Front and rear impact tests for the head restraints mounted on the bench type seat of light commercial vehicle have been realized on the linear impact test system in METU-BILTIR Center Vehicle Safety Unit.
- Image processing of the high-speed video recorded during the front and rear impact tests has been conducted.
- The complete head restraint model with the simplified seat model instead of the complex seat model has been developed.
- FEA for the front and rear impact tests of the head restraint mounted on the simplified seat model have been conducted.
- FEA results and linear impact test results have been compared and it is seen that they are in good agreement.
- FEA with different spring stiffness and damping coefficients which represent the seat-back reclining are realized. In FEA of the front impact, although the maximum acceleration values increase when spring stiffness coefficient (in the range of 50-500 N/mm) increases, the maximum acceleration values are quite below 80g which is the requirement of Annex 6 of UN ECE R17. In FEA of

the rear impact, the maximum acceleration values do not significantly change when spring stiffness coefficient (in the range of 50-500 N/mm) increases. In FEA of the front and rear impacts, the maximum acceleration values are not significantly affected when damping coefficient (in the range of 0-0.2 Ns/mm) increases for the same spring stiffness coefficient.

- In the finite element modelling of simplified seat model, seat-back and seat-base are defined as elastic. Later, FEA study has also been performed with defining seat-back and seat-base as rigid instead of elastic, however, the acceleration results have been obtained higher compared to the experimental results. Thus, it has been seen that the finite element modelling of the simplified seat with elastic seat-back and seat-base is appropriate.

Main contributions of the study can be summarized as follows:

- It can be stated that instead of using the complete head restraint model with the complex seat model, using the complete head restraint with the simplified seat model is sufficient in FEA studies.
- It is shown that head restraint manufacturers can use the proposed method and can be confident about success of the head restraint in the linear impact tests beforehand.

7.2. Suggestions for Further Studies

The study may be extended with the following studies:

- Different seat types other than bench type seat of light commercial vehicle can be studied.
- Different shapes, sizes, or mechanisms of the head restraints may be studied.
- Different material models in FEA may be studied for head restraints.
- For rear impact model, a different seat model can be used to include effect of seat stiffness in vertical direction in addition to the horizontal direction.

- For increasing sensitivity and decreasing solving time in FEA, mesh-dependency may be studied.

REFERENCES

[1] C. C. Chou, B. B. Fileta, T. B. Khalil, A. I. King, H. F. Mahmood, H. J. Mertz, J. Wismans, P. Prasad, and J. E. Belwafa, *Vehicle Crashworthiness and Occupant Protection*. Michigan: Automotive Applications Committee, 2004.

[2] M. C. Case and M. G. Lay, "Road vehicle design standards," in *Handbook of Transport Systems and Traffic Control* (K. J. Button and D. A. Hensher, eds.), vol. 3, pp. 387–398, Emerald Group Publishing Limited, 2001.

[3] D. Vashist and N. Kumar, "A review of active and passive automotive safety systems," *International Journal OF Engineering Sciences & Management Research*, vol. 4, no. 4, p. 8, 2017.

[4] U. Doğan, "Effect of strain history on simulation of crashworthiness of a vehicle," M.S. thesis, Middle East Technical University, Ankara, Turkey, 2009.

[5] R. Nayak, R. Padhye, K. Sinnappoo, L. Arnold, and B. K. Behera, "Airbags," *Textile Progress*, vol. 45, no. 4, pp. 209–301, 2013.

[6] M. I. Kiron, "Airbag for automobiles: Material, properties, working principle, production." https://textilelearner.net/airbag-for-automobiles/. (Accessed: 12.01.2023).

[7] K. L. M.G.C. Rekveldt, "Literature survey on in-vehicle safety devices," Tech. Rep. 03.OR.BV.037.1/MRE, TNO report, 2022. https://citeseerx.ist.psu.edu/viewdoc/download?doi=10.1.1.129.6700&rep=rep1&type=pdf.

[8] E. NCAP, "Euro NCAP improves tertiary safety by introducing a mobile app for first responders in europe | euro NCAP." https://www.euroncap.com/en/press-media/press-releases/. (Accessed: 2023-01-03).

[9] "Vehicle regulations." https://unece.org/transport/vehicle-regulations. (Accessed: 2023-02-21).

[10] "Regulations NHTSA." https://www.nhtsa.gov/laws-regulations/fmvss. (Accessed: 2023-02-21).

[11] "Euro NCAP." https://www.euroncap.com/en. (Accessed: 2023-02-21).

[12] "Global NCAP." https://www.globalncap.org/. (Accessed: 2023-02-21).

[13] "UN regulations (addenda to the 1958 agreement) | UNECE." https://unece.org/un-regulations-addenda-1958-agreement. (Accessed: 2023-02-21).

[14] "List of chinese standard." https://www.chinesestandard.net/StandardList.aspx. (Accessed: 2023-05-23).

[15] "Anthropomorphic test devices (ATD)." https://www.humaneticsgroup.com/products/anthropomorphic-test-devices. (Accessed: 2023-12-15).

[16] S. S. Karadeniz, "Desing, analysis and experimental study of a novel side thoras impactor to be used in pedestrian protection tests for flat front vehicles," Ph.D dissertation, Middle East Technical University, Ankara, Turkey, 2021.

[17] T. Xu, X. Sheng, T. Zhang, H. Liu, X. Liang, and A. Ding, "Development and validation of dummies and human models used in crash test," *Applied Bionics and Biomechanics*, vol. 2018, p. e3832850, 2018-11-13. Publisher: Hindawi.

[18] *Regulation No. 17. Uniform provisions concerning the approval of vehicles with regard to the seats, their anchorages and any head restraints*. UN ECE.

[19] A. Patil and U. Patil, "Overview of automotive seating system," *International Journal of Engineering Research and General Science*, vol. 5, no. 6, pp. 6–14, 2017.

[20] H. N. Kale and C. L. Dhamejani, "Design parameters of driver seat in automobile," *International Journal of Research in Engineering and Technology*, vol. 4, no. 6, pp. 448–452, 2015.

[21] F. Li, N.-s. Liu, H.-g. Li, B. Zhang, S.-w. Tian, M.-g. Tan, and B. Sandoz, "A review of neck injury and protection in vehicle accidents," *Transportation Safety and Environment*, vol. 1, no. 2, pp. 89–105, 2019.

[22] D. C. Viano, "Seat design principles to reduce neck injuries in rear impacts," *Traffic Injury Prevention*, vol. 9, no. 6, pp. 552–560, 2008.

[23] B. D. Stemper, N. Yoganandan, and F. A. Pintar, "Effect of head restraint backset on head–neck kinematics in whiplash," *Accident Analysis & Prevention*, vol. 38, no. 2, pp. 317–323, 2006.

[24] *FMVSS No. 202 Head Restraints For Passenger Vehicles*. NHTSA.

[25] Research Council for Automobile Repairs, *RCAR-IIWPG Seat/Head Restraint Evaluation Protocol (Version 3)*. (Accessed: 04.10.2023).

[26] A. L. Young, B. T. Ragel, E. Su, C. N. Mann, and E. H. Frank, "Assessing automobile head restraint positioning in portland, oregon," *Injury Prevention*, vol. 11, no. 2, pp. 97–101, 2005.

[27] J. Taylor, J. Burke, J. Gavencak, and P. Panwar, "Knowledge and application of correct car seat head restraint usage among chiropractic college interns: a cross-sectional study," *The Journal of the Canadian Chiropractic Association*, vol. 49, no. 1, pp. 32–39, 2005.

[28] U. Göçmen, "Experimental whiplas analysis with hybrid III 50 percentile test dummy," M.S. thesis, Middle East Technical University, Ankara, Turkey, 2009.

[29] "Gallatin valley chiropractic: Bozeman, MT: Back and neck pain, whiplash & more." `https://www.gallatinvalleychiropractic.com/whiplash-mechanism-and-phases`. (Accessed: 2023-09-20).

[30] M. Özdemir, "Analysis of whiplash during rear crash and development of an anti-whiplash seat mechanism," Ph.D dissertation, Middle East Technical University, Ankara, Turkey, 2013.

[31] M. Acar and S. Bewsher, "Design concepts for an integrated whiplash mitigating head restraint and seat," *International Journal of Crashworthiness*, vol. 21, no. 1, pp. 79–88, 2016.

[32] B. Lundell, L. Jakobsson, B. Alfredsson, M. Lindström, and L. Simonsson, "The WHIPS seat a car seat for improved protection against neck injuries in rear-end impacts," in *16th International Technical Conference on the Enhanced Safety of Vehicles*, (Windsor, Canada), pp. 0–8, 1998.

[33] K.-U. Schmitt, M. Muser, M. Heggendorn, P. Niederer, and F. Walz, "Seat component to prevent whiplash injury," in *Proceedings of the 18th International Technical Conference on the Enhanced Safety of Vehicles*, (Nagoya, Japan), p. 6p, National Highway Traffic Safety Administration, 2003.

[34] *MADYMO*. `https://plm.sw.siemens.com/en-US/simcenter/mechanical-simulation/madymo/`.

[35] M. Luo and Q. Zhou, "A vehicle seat design concept for reducing whiplash injury risk in low-speed rear impact," *International Journal of Crashworthiness*, vol. 15, no. 3, pp. 293–311, 2010. Publisher: Taylor & Francis _eprint: https://doi.org/10.1080/13588260903335282.

[36] X. Zhang and Q. Zhou, "An energy-absorbing sliding seat for reducing neck injury risks in rear impact—analysis for prototype built," *Traffic Injury Prevention*, vol. 17, pp. 313–319, 2016. Publisher: Taylor & Francis.

[37] M. Özdemir, S. K. İder, and M. Gökler, "Experimental and numerical investigation of comparability of whiplash sled test results," *Journal of the Brazilian Society of Mechanical Sciences and Engineering*, vol. 38, no. 2, pp. 395–402, 2016.

[38] K. Wiklund and H. Larsson, "Saab active head restraint (SAHR) - seat design to reduce the risk of neck injuries in rear impacts," SAE Technical Paper 980297, SAE International, Warrendale, PA, 1998. ISSN: 0148-7191, 2688-3627.

[39] M. Acar, S. J. Clark, and R. Crouch, "Smart head restraint system," *International Journal of Crashworthiness*, vol. 12, no. 4, pp. 429–435, 2007. Publisher: Taylor & Francis _eprint: https://doi.org/10.1080/13588260701483367.

[40] O. S. A. A. Laban, "Modelling of whiplash trauma; parametric study of rear-end collision and development of head restraint system," M.S. thesis, Qatar University, Doha, Qatar, 2017.

[41] M. Chen, L. Zhou, Z. Meng, X. Wei, and H. Wang, "The effects of packaging on collision energy absorption of automotive seat headrest," *MATEC Web of Conferences*, vol. 65, p. 01008, 2016.

[42] D. Devkate and N. L.G., "Study of influence of different parameters of head-restraints on energy absorption test," *International Journal of Innovative Research in Advanced Engineering*, vol. 2, 2015.

[43] E. R. Naber and M. E. Carley, "Expanded polypropylene foam as an effectives-olution to passing fmvss 202a," in *SAE 2006 World Congress & Exhibition*, pp. 2006–01–1473, 2006.

[44] R. Çöl, "Developing of systems to evaluate child seat and restraint systems according to ECE r44," M.S. thesis, Middle East Technical University, Ankara, Turkey, 2012.

[45] K. Özden, "Investigation of reducing run time in vehicle level finite element analyses for curtain airbag development," M.S. thesis, Middle East Technical University, Ankara, Turkey, 2012.

[46] S. Kaya, "Developing test procedure and design of fixture for dymanic test of road ambulances," M.S. thesis, Middle East Technical University, Ankara, Turkey, 2019.

[47] *Operation Manual METU E-Liner PED LEG*. FronTone Automotive.

[48] *Motion Analysis - TEMA & TrackEye - Image Systems*. `https://imagesystems.se/`.

[49] A. Chelikani, "Simulation of a backrest moment test for an automotive front seat using nonlinear contact finite element analysis," master of science, Clemson University, Ann Arbor, United States, 2007. ISBN: 9780549158943.

[50] G. Vemulakonda, B.-R. Tang, R. Jayachandran, D. Wan, S.-G. Thakurta, J. M. Chang, T. Tyan, J. Cheng, J. Doong, L. Shaner, and D. Bhalsod, "Approaches to modeling the dynamic interaction for an automotive seat and occupant system," *Journal of Passenger Cars: Mechanical Systems Journal*, vol. 116, no. 6, pp. 1038–1050, 2007.

[51] *Ansys LS-DYNA | Crash Simulation Software*. https://www.ansys.com/products/structures/ansys-ls-dyna.

[52] *Pam-Crash*. https://www.esi-group.com/pam-crash.

[53] H. Zhang, S. Raman, M. Gopal, and T. Han, "Evaluation and comparison of CFD integrated airbag models in LS-DYNA, MADYMO and PAM-CRASH," in *SAE 2004 World Congress & Exhibition*, pp. 2004–01–1627, 2004.

[54] K. Solanki, D. L. Oglesby, C. L. Burton, H. Fang, and M. F. Horstemeyer, "Crashworthiness simulations comparing PAM-CRASH and LS-DYNA," in *SAE 2004 World Congress & Exhibition*, pp. 2004–01–1174, 2004.

[55] *Ansys SpaceClaim | 3D CAD Modelling Software*. https://www.ansys.com/products/3d-design/ansys-spaceclaim.

[56] K. Ramaswamy, B. Patham, V. Savic, and B. Tripathy, "Stable and accurate LS-DYNA simulations with foam material models: Optimization of finite element model parameters," *SAE International Journal of Materials and Manufacturing*, vol. 10, no. 2, pp. 226–233, 2017-03-28.

[57] V. Srivastava and R. Srivastava, "Performance evaluation of fu chang and low density foam model for expanded polypropylene," *MIT International Journal of Mechanical Engineering*, vol. 4, no. 1, pp. 49–53, 2014.

[58] M. Avalle, G. Belingardi, and R. Montanini, "Characterization of polymeric structural foams under compressive impact loading by means of energy-absorption diagram," *International Journal of Impact Engineering*, vol. 25, no. 5, pp. 455–472, 2001.

[59] Y. Y. Tay, C. S. Lim, and H. M. Lankarani, "A finite element analysis of high-energy absorption cellular materials in enhancing passive safety of road vehicles in side-impact accidents," *International Journal of Crashworthiness*, vol. 19, no. 3, pp. 288–300, 2014.

[60] B. Sambamoorthy and T. Halder, "Characterization and component level correlation of energy absorbing (EA) polyurethane foams (PU) using LS-DYNA material models," in *3rd European LS-DYNA Conference*, p. 8, DYNAlook, 2001.

[61] *LS-DYNA Keyword User's Manual Volume II*. (Accessed: (17.07.2023)[Online].

[62] S. D. Burbank and L. V. Smith, "Dynamic characterization of rigid foam used in finite element sports ball simulations," *Proceedings of the Institution of Mechanical Engineers, Part P: Journal of Sports Engineering and Technology*, vol. 226, no. 2, pp. 77–85, 2012.

[63] A. Škrlec and J. Klemenc, "Estimating the strain-rate-dependent parameters of the cowper-symonds and johnson-cook material models using taguchi arrays," *Strojniški vestnik - Journal of Mechanical Engineering*, vol. 62, no. 4, pp. 220–230, 2016.

[64] "Hex mesh vs tet mesh (which is better and why?." `https://engineeryoursound.com/hex-mesh-vs-tet-mesh-which-is-better-and-why/`. (Accessed: 2023-11-24).

[65] *Contact types*. (Accessed: 29.06.2023)[Online].

APPENDICES

A. LINEAR IMPACT TEST SYSTEM IN METU-BILTIR CENTER VEHICLE SAFETY UNIT

The linear impact test system in METU-BILTIR Center Vehicle Safety Unit has been given in Figure 2.1 and some technical details are given in Table A.1.

Table A.1. Some Technical Details of the Used Linear Impact Test System

Power	Solely electrically driven
Acceleration limit	120 m/s^2
Speed range	1-42 km/h
Speed accuracy	$\pm$ 0.1 km/h
Repeatability	$\pm$ 0.1 km/h
Targeting Precision	Within a radius of 5 mm
Max. Impactor Mass	35 kg
Max. Impactor Mass at 42.0 km/h	13.5 kg at $+5^o$ vertical
Max. Impactor height	2025 mm
Min. Impactor height	540 mm

B. TEST FIXTURE USED IN LINEAR IMPACT TEST SYSTEM

There are two types of test fixtures for the front and rear impact tests. Front impact test fixture has the dimensions of 650 mm x 750 mm with the thickness of 15 mm. There are two handles and some seat mounting parts on the fixture. Overall dimensions of the front impact test fixture are shown in Figure B.1 Rear impact test fixture is manufactured with using 40 mm x 40 mm square profiles. This fixture is used to provide 30^{o} angle to the seat during the tests. The seat is mounted on the front impact test fixture and the front impact test fixture is mounted on rear impact text fixture for rear impact tests. Overall dimensions of the rear impact test fixture are shown in Figure B.2.

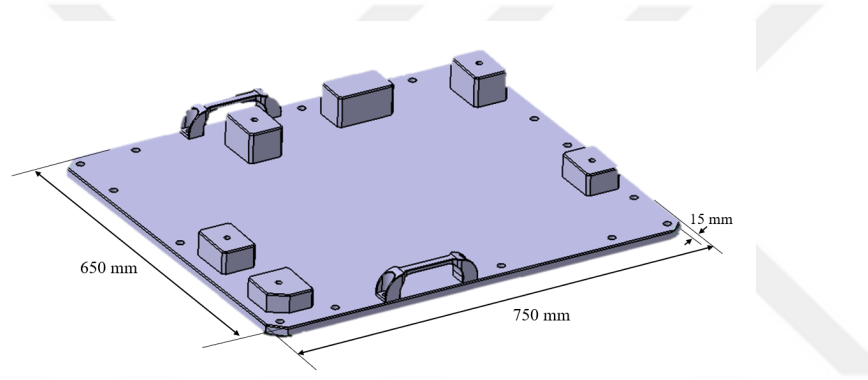

Figure B.1. Overall dimensions of front impact test fixture

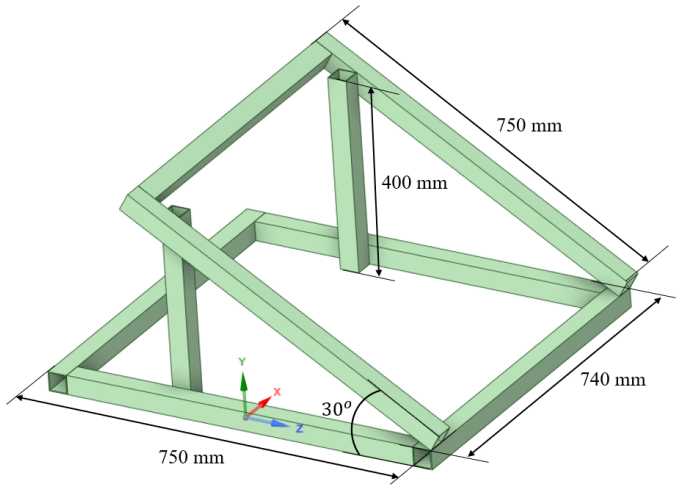

Figure B.2. Overall dimensions of rear impact test fixture